Optical Specifications for the MMT Conversion

Daniel Fabricant
Brian McLeod
Steve West
December 21, 1999

VERSION 7

Contents

1 Introduction

1.1 Purpose of this Document

This document is meant to define the error budgets for the fabrication and collimation of the optics for the converted MMT. Important background information can be found in a number of publications and technical memoranda; these are listed in section 10 below. In the case of a conflict between the references and the present specifications, the latter shall prevail.

1.2 The 6.5m MMT

The Smithsonian Institution and the University of Arizona are undertaking the conversion of the Multiple Mirror Telescope (MMT) to a telescope with a single 6.5 meter diameter primary mirror. All of the MMT optics will be replaced in the conversion, and the converted telescope will have a classical Cassegrain optical design with a parabolic primary and hyperbolic secondary. Three secondary mirrors will be provided for the converted MMT, yielding nominal focal ratios of f/5, f/9 and f/15. A refractive corrector can be installed at the f/5 focus to produce a very wide field, the f/9 focus will accommodate the current instruments and the f/15 will be used for the IR and for adaptive optics. These foci in combination will give the converted MMT an unsurpassed versatility.

1.3 Outline

We begin with optical and mechanical specifications for the telescope optics in sections 2 and 3. Then we define the criteria used to evaluate the optical performance of the system. In section 5 we present the error budgets for the various configurations of the telescope. The following two sections give the specifications for fabrication and collimation that are required to meet the error budgets. We conclude with a discussion of thermal and wind effects in section 8.

2 Optical Prescriptions

2.1 Introduction to the Optics

Here we list the optical prescriptions for the various configurations of the telescope. Figure 1 shows the layout of the optics.

The Primary

	Diameter	Radius of Curvature	Conic Constant
Spec	6502 mm	16256±2.5 mm	–1.0000±0.00025
As built		16255.3±0.3 mm	$-1.0000^{+0.0001}_{-0.0004}$

The Bare Cassegrain Foci

f/	Scale (mm/arcsec)	Back Focal Distance (mm)	Foc Surf Rad Curv (mm)	Secondary Conic	Secondary Vert Rad (mm)
5.16	0.162	1851±4	2163	–2.6946	5151.3
9.00	0.284	1778±43	1273	–1.7492	2805.8
15.00*	0.463	2286±104	849	–1.4091	1794.5

∗ f/15 secondary is undersized from an f/14.6 parent.

The Wide-Field Cassegrain Foci (with refractive corrector)

f/	Purpose	ADC?	Scale (mm/arcsec)	Distortion	Focal Surface Radius (mm)	Focal Surface Conic
5.29	Spectroscopy, 1° FOV	Yes	0.167	1.8%	3404	–665
5.36	Imaging, 0.5° FOV	No	0.169	1%	Flat	

Field Diameters vs. Image Quality (on appropriately curved focal surfaces)

f/		0.25 arcsec (RMS dia)	0.5 arcsec (RMS dia)	1.0 arcsec (RMS dia)	Unvignetted Field
5.16	bare	2′	5′	9′	>60′
9.00	bare	7′	13′	23′	12′
15.00	bare	13′	20′	29′	6′
5.29	cor.	18′	60′	67′	>60′
5.36	cor.	34′	39′	44′	>30′

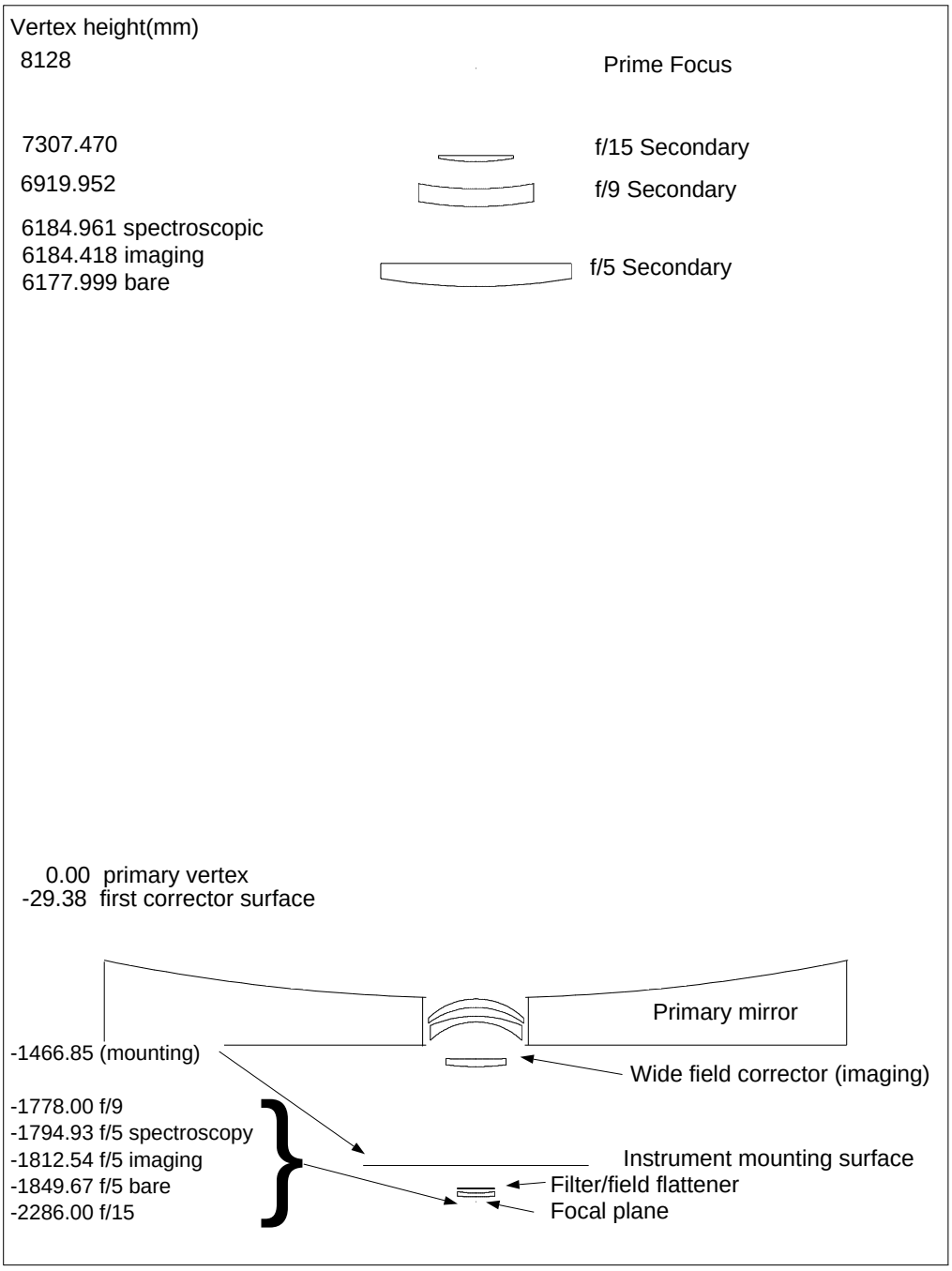

Figure 1: Layout of the optics, including all three secondaries and the imaging configuration of the wide-field corrector.

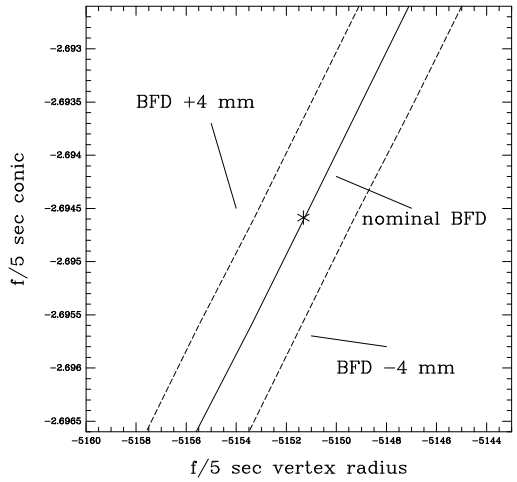

Figure 2: Allowable ranges on f/5 secondary conic and radius, set by allowing a ±4mm range on the back focal distance.

2.2 f/5 Bare

The f/5 secondary design was driven by the requirements of the wide field corrector, subject to the constraint that the bare system (without corrector) has classical Cassegrain optics. The back focal distance of the bare system is several cm larger than that of the corrected system. The clear apertures are derived by requiring a 1° diameter unvignetted field with the corrector in place (spectroscopy configuration). The conic/radius error specification is shown in Figure 2. Details of the f/5 secondary specifications are described by Fabricant (1999).

Secondary Vertex Radius	Secondary Conic	Secondary Clear Aperture
–5151.322 mm	–2.6946	1688 mm
–202.8080 in		66.46 in

In the following table, the back focal distance and primary–secondary separation are chosen to produce a perfect on-axis image. With these parameters fixed, the focal surface radius of curvature that provides the best off-axis images is determined.

Back Focal Distance	Primary–Secondary Separation	Focal Surface Radius of Curvature
1849.67 mm	6178.00 mm	–2163 mm
72.821 in	243.228 in	–85.16 in

2.3 f/5 With Wide Field Refractive Corrector

2.3.1 Spectroscopic configuration

File : spect_final.ZMX
Title: MMT Spectroscopic Corrector - As Built
Date : FRI SEP 17 1999

Surf	Type	Radius	Thickness	Glass	Diameter	Conic	Vertex Height
OBJ	STANDARD	Infinity	Infinity		0	0	
STO	STANDARD	-16256	-6184.961	MIRROR	6502.4	-1	0.000
2	STANDARD	-5150.974	6184.961	MIRROR	1683.504	-2.6946	-6184.961
3	STANDARD	Infinity	29.382		818.3793	0	0.000
4	STANDARD	604.737	73.288	SIL5C	831.44	0	29.382
5	STANDARD	694.826	80.085		831.44	0	102.670
6	STANDARD	1012.496	46.741	SIL5C	797.03	0	182.755
7	STANDARD	577.816	171.25		797.03	0	229.496
8	STANDARD	-5983.1	49.108	SIL5C	767.41	0	400.746
9	STANDARD	-2104.29	53.828		767.41	0	449.854
10	COORDBRK	-	0	-	-	-	503.682
11	FZERNSAG	Infinity	25.4	SFSL5Y_5C	748.92	0	503.682
12	FZERNSAG	Infinity	0.127	CAF2P20	748.92	0	529.082
13	FZERNSAG	Infinity	15.24	PBL6Y_5C	748.92	0	529.209
14	STANDARD	Infinity	25.705		748.72	0	544.449
15	COORDBRK	-	0	-	-	-	570.154
16	FZERNSAG	Infinity	15.24	PBL6Y_5C	748.92	0	570.154
17	FZERNSAG	Infinity	0.127	CAF2P20	748.92	0	585.394
18	FZERNSAG	Infinity	25.4	SFSL5Y_5C	748.92	0	585.521
19	STANDARD	Infinity	699.754		748.92	0	610.921
20	COORDBRK	-	0	-	-	-	1310.675
21	STANDARD	Infinity	12.7	SIL5C	648.5093	0	1310.675
22	STANDARD	Infinity	471.551		647.8104	0	1323.375
IMA	STANDARD	-3404			611.1694	-665	1794.926

2.3.2 Imaging configuration

File : image_final.ZMX
Title: MMT Imaging Corrector - As Built
Date : FRI SEP 17 1999

Surf	Type	Radius	Thickness	Glass	Diameter	Conic	Vertex height
OBJ	STANDARD	Infinity	Infinity		0	0	
STO	STANDARD	-16256	-6184.419	MIRROR	6502.4	-1	0.000
2	STANDARD	-5150.974	6184.419	MIRROR	1714.5	-2.6946	-6184.419
3	STANDARD	Infinity	29.382		621.7533	0	0.000
4	STANDARD	604.737	73.288	SIL5C	831.44	0	29.382
5	STANDARD	694.826	80.085		831.44	0	102.670
6	STANDARD	1012.496	46.741	SIL5C	797.03	0	182.755
7	STANDARD	577.816	325.001		797.03	0	229.496
8	STANDARD	-8055.3	66.097	SIL5C	523.95	0	554.497
9	STANDARD	-2020.77	1044.671		523.95	0	620.594
10	STANDARD	Infinity	8.467	S-TIL1	365.1734	0	1665.265
11	STANDARD	Infinity	38.1		364.3608	0	1673.732
12	STANDARD	-1134.801	48.26	SIL5C	360.8682	0	1711.832
13	STANDARD	-4097.612	52.445		360.8158	0	1760.092
IMA	STANDARD	Infinity			358.5954	0	1812.537

2.4 f/9

Here we require a 12′ unvignetted field.

Secondary Vertex Radius	Secondary Conic	Secondary Minimum Clear Aperture	Secondary Design Clear Aperture
–2805.788 mm	-1.749220	997.20 mm	1006.7 mm
–110.464100 in		39.259 in	39.64 in

Back Focal Distance	Primary–Secondary Separation	Focal Surface Radius of Curvature
1778.000 mm	6919.952 mm	–1273 mm
70.000 in	272.4391 in	–50.12 in

2.5 f/15

Here the secondary is undersized from a f/14.6 parent so that the aperture stop is at the secondary mirror. See section 9.1 below for a discussion of infrared performance. The f/15 issues are also discussed in detail in John Hill's LBT Technical Memo "Infrared Secondaries: The Meaning of F/15", dated September 29, 1993. The prescription was updated in November 1994 by John Hill, Matt Johns and George Rieke. The secondary diameter given below should be regarded as preliminary.

Secondary Vertex Radius	Secondary Conic	Secondary Diameter
–1794.5486mm	–1.40911	642.05 mm
–70.6515in		25.278 in

Back Focal Distance	Primary–Secondary Separation	Focal Surface Radius of Curvature
2286.0 mm	7307.470 mm	–864 mm
90.000 in	287.6956 in	–34.0 in

3 Mechanical Description of the Optical Elements

3.1 Optical Materials

We use six different optical materials for the MMT Conversion: (1) Ohara E6 (a borosilicate glass) for the primary, (2) Schott Tempax (a borosilicate glass) for the f/9 secondary, (3) Zerodur for the f/5 secondary, (4) fused silica for the wide-field corrector, (5) Ohara FSL5Y and (6) Ohara PBL6Y; FSL5Y and PB6LY are used for the ADC prisms in the wide-field corrector. Some representative mechanical properties near 25 °C are given in the following table.

Material	Density (g/cc)	Young's Modulus (MPa)	Poisson's Ratio	Coefficient of Thermal Expan.* (per °C)	Thermal Conductivity (watts/m^2–°C)
Ohara E6	2.18	57,500	0.195	2.9×10^{-6}	0.96
Tempax borosilicate	2.23	63,000	0.2	3.2×10^{-6}	1.16
Zerodur	2.53	90,600	0.24	$2–4\times10^{-8}$	1.65
fused silica	2.202	73,000	0.17	5.2×10^{-7}	1.38
Ohara FSL5Y	2.46	62,300	0.227	9.0×10^{-6}	1.01
Ohara PBL6Y	2.46	60,500	0.205	8.3×10^{-6}	1.02

* The tabulated CTE's are averaged over different temperature ranges. For the Ohara materials, the range is -30 to +70 °C. For Zerodur the range is 0 to 50 °C, and refers to measurements of samples from the f/5 secondary. For fused silica the range is 5 to 35 °C.

3.2 Primary and Secondary Dimensions

Element	Drawing Number	Clear Diameter (mm)	Overall Diameter (mm)	Edge Thick. (mm)	Center Thick (mm)	Weight (kg)
Primary	S0 1168	6502	6512	711	391	7735
f/5 Secondary	SAO MMTC-001	1692	1715	133	206	288
f/9 Secondary	Hextek 10/15/90	1007	1022	152	152	77
f/15 Secondary						

3.3 Wide Field Corrector Element Dimensions

Element	Drawing Number	Clear Diameter (mm)	Overall Diameter (mm)	Center Thick (mm)	Weight (kg)
Lens 1	SAO MMTC-1000	806 mm	831 mm	73	73
Lens 2	SAO MMTC-1001	772 mm	797 mm	47	93
Lens 3	SAO MMTC-1002	728 mm	767 mm	49	39
Lens 4	SAO MMTC-1003	484 mm	524 mm	66	28
Top ADC Assembly	SAO MMTC-500	724 mm	749 mm	41	45
Bottom ADC Assembly	SAO MMTC-501	724 mm	749 mm	41	45
Element	Drawing Number	Clear Diameter (mm)	Overall Diameter (mm)	Min. Thick. (mm)	Max. Thick (mm)
ADC Prism 1	SAO MMTC-1004	724 mm	749 mm	18.2	32.6
ADC Prism 2	SAO MMTC-1005	724 mm	749 mm	8.7	21.8
ADC Prism 3	SAO MMTC-1006	724 mm	749 mm	8.4	22.1
ADC Prism 4	SAO MMTC-1007	724 mm	749 mm	17.9	32.9

3.4 Wide Field Corrector Assembly

Configuration	Drawing Number	Weight (kg)
Spectroscopic Mode	SAO MMTC-504	606
Imaging Mode	SAO MMTC-505	467

4 Evaluation Criteria for Optical Performance

4.1 The Structure Function

Angel (1987) has outlined the error budget strategy we adopt for the converted MMT. Since our goal is to build a telescope which degrades the incoming image as little as possible, it seems appropriate to specify the errors in the telescope so they correspond to the distortions already induced by the atmosphere. The root mean square wavefront difference introduced by the atmosphere between points on the wavefront with spatial separation x is:

$$\delta\phi = 0.4175 * (x/r_0)^{5/6} \tag{1}$$

where the error is expressed as phase difference, $\delta\phi$, in waves. No matter what value of r_0 we use, the errors are always proportional to $x^{5/6}$ as long as the atmosphere retains a Kolmogorov spectrum. This allows us to relax the tolerance on the telescope optics and alignment at large scales since the atmosphere has already distorted the wavefront. We have adopted the "structure function" to describe the error in the incoming wavefront as a function of separation. Thus, by selecting a particular value of r_0, we may specify the permissible wavefront distortion introduced by a mirror or a telescope. Converting from phase error to a linear dimension, we find the structure function:

$$\delta^2(x) = \left(\frac{\lambda}{2\pi}\right)^2 6.88 \left(\frac{x}{r_0}\right)^{5/3} \tag{2}$$

Tilt Compensation Since any tilt present in the primary or secondary optics can be removed simply by tilting the element, we do not include tilt in the structure function. Removing the mean tilt from the wavefront rolls off the structure function at large spatial scales:

$$\delta^2(x) = \left(\frac{\lambda}{2\pi}\right)^2 6.88 \left(\frac{x}{r_0}\right)^{5/3} \left[1 - 0.975 \left(\frac{x}{D}\right)^{1/3}\right] \tag{3}$$

where D is the telescope aperture diameter.

Scattering Effects Diffraction effects allow us to relax the specifications at small spatial scales. Ruze (1966) gives the fractional loss due to scattering from small errors on scales much less than r_0 as:

$$loss = \left(\frac{2\pi\sigma}{\lambda}\right)^2 \tag{4}$$

where σ is the rms deviation from the mean wavefront. We want to specify the small scale (1 cm) surface roughness so that no more than 3% of the light is scattered outside

the seeing disk at 350 nm from either the primary or secondary. To achieve this level of performance, $\sigma = 9.6$ nm, which implies a 13.6 nm rms wavefront difference or a 7 nm rms surface error. The overall wavefront error budget can then be specified as the structure function:

$$\delta^2(x) = 2\sigma^2 + \left(\frac{\lambda}{2\pi}\right)^2 6.88 \left(\frac{x}{r_0}\right)^{5/3} \tag{5}$$

$\delta(x)$ is the rms wavefront difference between points separated by x.

Zenith Angle When the telescope is looking away from the zenith, we may expect the images to degrade. The seeing degrades according to $(cos\, z)^{3/5}$, so an $r_0 = 45$ cm atmosphere will be only $r_0 = 30$ cm at a zenith angle, z, of 60°. We will allow the error budget for the primary mirror to relax in this same fashion. In principle, we could allow the error budget for the entire optical system relax in this manner, but there seems to be no compelling reason to do so.

4.2 Encircled Energy

We can also characterize the performance of the optical system based on the size of the image produced.

For a 2D Gaussian image, defined by:

$$\frac{1}{2\pi\sigma^2} exp\left[-0.5\left(\frac{r}{\sigma}\right)^2\right] \tag{6}$$

the power within a radius r in cylindrical coordinates is given by:

$$1 - exp\left[-0.5\left(\frac{r}{\sigma}\right)^2\right], \tag{7}$$

and we obtain the following equivalent measures of image size:

- 1.00″ FWHM
- 1.00″ 50% encircled energy diameter
- 1.28″ 68% encircled energy diameter (2D RMS image diameter)
- 1.52″ 80% encircled energy diameter
- 1.82″ 90% encircled energy diameter

- 10.1 cm r_0 ($0.5\mu m$) wavefront

In the general case images are non Gaussian, so a single number such as FWHM or RMS image diameter is not an adequate characterization. In most cases below we will specify the image quality in terms of the 90% encircled diameter. For historical reasons, some of the specifications are given in terms of another quantity. In those cases will use the above relations as an approximate conversion.

4.3 Differential Distortion

For wide-field imaging and spectroscopy another limitation is imposed on the optical system. The distortion pattern must be circularly symmetric about the center of the focal plane so that images remain at a fixed radius in the focal plane as the instrument rotator tracks. In the presence of misalignments in the system this is not guaranteed. We define the "differential distortion" as follows. Let A be the spherical field angle that produces an image, a, with its centroid on the optical axis of the instrument rotator. Let B be the locus of all field angles such that $|B - A|$ is constant. The centroid of B is located at position b in the focal plane. The differential distortion is defined as $max(b - a) - min(b - a)$. We will discuss below the specific tolerances on the differential distortion.

4.4 Optical Axis Deviation

In a perfectly aligned system, an object on the optical axis of the primary will be imaged to the center of the focal plane. (By the center of the focal plane we mean on the axis of the instrument rotator.) In a misaligned system this will not necessarily be the case. If the pointing direction of the telescope were defined in terms of the primary mirror axis, this would lead to guiding errors as the instrument rotator rotated about one axis and the telescope tracked about another. It is straightfoward, and standard practice, to add offsets to the pointing direction so that it coincides with the rotator axis. In fact, it is not obvious that one could easily determine where the axis of any element of the telescope, other than the rotator, intersects the focal plane. In our analysis of encircled energy, for reasons of simplicity, we do measure all field angles with respect to the primary axis. Unless the axis deviations are substantial compared with the maximum field angle, this should not cause any complications. In no case does the offset become large before the image quality deteriorates unacceptably. Thus, the tolerances on the offset of the axis of any element is dictated only by image quality and differential distortion.

5 Optical Performance Goals

The performance goals vary by focus; performance appropriate for the bare Cassegrain foci will be unachievable over a 1° field with the wide field corrector. In much of what follows in this section, we follow the lead of John Hill, who has developed the specifications for the LBT. We refer the reader to his memos for the unexpurgated version. A major difference between John's LBT specifications and the current MMT specifications is that we have emphasized the requirements of the wide field, which drive some of the optical specifications.

5.1 Goals for the Bare Cassegrain Foci

For the bare Cassegrain foci, the optical error budget for the converted MMT is specified to match the wavefront produced by the atmosphere in the very best seeing conditions. Specifically, the goal is to have the telescope produce a wavefront structure function equivalent to an $r_0 = 45$ cm atmosphere at a wavelength of 5000 Å, or images of $\sim 0.23''$ FWHM. The telescope and atmosphere (during superlative seeing) should deliver a wavefront to the focal plane equivalent to an $r_0 = 32$ cm atmosphere or a detected image of $0.32''$ FWHM.

5.2 Telescope Error Budget–Bare Cassegrain Foci

Error Source	Image FWHM (arcseconds)	Equivalent r_0 (cm)
Tracking and Drives	0.070	∼144
Secondary Alignment and Focus	0.090	∼112
Primary Mirror Surface	0.170	∼59
Primary Conic/Radius	0.056	∼180
Secondary Mirror Surface	0.040	∼253
Secondary Conic/Radius	0.028	∼361
Telescope Seeing (5%)	0.060	∼168
Best Atmospheric Seeing	0.225	∼45
Best Final Image (total)	0.319	∼32

5.3 Specifications for the F/5 Wide Field

5.3.1 Introduction to the Wide Field Specifications

The wide field specifications must consider several additional error terms: (1) the design optical performance of the corrector, (2) corrector fabrication errors and (3) corrector collimation. For the wide field we adopt geometrical optics specifications for the encircled energy diameters. supplemented by a lateral color specification. Fortunately, the lateral color is unaffected by collimation errors and so we defer the lateral color specifications to the section on corrector fabrication tolerances.

In addition to the image quality specifications, we need to specify: differential image distortion (which will cause positioning errors and light loss with optical fibers), and surface roughness (which will cause light loss due to scattering).

5.3.2 Performance of Perfect Corrector Optics

We first describe the performance of the wide field system with a perfect primary and secondary mirror and "as-designed" corrector optics.

Performance with Perfect Optics

Spectroscopic Configuration–Run 121796AV

Lateral Color Shifts in μm

Field Angle	3300Å	3500Å	4000Å	4775Å	6772Å	10000Å	3300-10000Å
$0'$	0	0	0	0	0	0	0
$15'$	-36	-27	-12	0	12	20	56
$24'$	-24	-17	-7	0	4	5	29
$30'$	10	10	7	0	-16	-26	-37

Diameter to Encircle 50% of the Energy (in μm)

Field Angle	3300Å	3500Å	4000Å	4775Å	6772Å	10000Å
$0'$	8	7	6	8	9	11
$15'$	36	36	39	41	41	44
$24'$	34	35	36	39	41	45
$30'$	83	80	74	72	66	67

Diameter to Encircle 80% of the Energy (in μm)

Field Angle	3300Å	3500Å	4000Å	4775Å	6772Å	10000Å
$0'$	38	32	21	11	13	15
$15'$	51	53	57	62	64	68
$24'$	53	54	57	61	66	71
$30'$	105	101	93	91	89	90

Diameter to Encircle 90% of the Energy (in μm)

Field Angle	3300Å	3500Å	4000Å	4775Å	6772Å	10000Å
$0'$	49	42	30	21	15	16
$15'$	57	58	64	69	74	79
$24'$	64	64	67	69	74	79
$30'$	120	115	108	105	107	112

Performance with Perfect Optics

Imaging Configuration–Run 121896AR

Lateral Color Shifts in μm

Field Angle	3300Å	3500Å	4000Å	4775Å	6772Å	10000Å	3300-10000Å
$0'$	0	0	0	0	0	0	0
$8.75'$	-12	-9	-4	0	3	4	16
$14'$	-7	-4	-1	0	-1	-4	-7
$17.5'$	6	6	4	0	-8	-16	-22

Diameter to Encircle 50% of the Energy (in μm)

Field Angle	3300Å	3500Å	4000Å	4775Å	6772Å	10000Å
$0'$	6	2	6	10	15	15
$8.75'$	15	11	7	7	8	10
$14'$	13	11	9	9	14	18
$17.5'$	15	14	12	12	17	20

Diameter to Encircle 80% of the Energy (in μm)

Field Angle	3300Å	3500Å	4000Å	4775Å	6772Å	10000Å
$0'$	16	8	9	14	19	20
$8.75'$	23	19	13	10	11	14
$14'$	21	18	14	16	22	28
$17.5'$	23	22	20	19	22	29

Diameter to Encircle 90% of the Energy (in μm)

Field Angle	3300Å	3500Å	4000Å	4775Å	6772Å	10000Å
$0'$	23	15	9	15	20	22
$8.75'$	41	32	19	14	13	16
$14'$	41	31	20	20	25	32
$17.5'$	28	26	25	23	25	33

5.3.3 Wide Field Error Budget

For the purpose of the specifications, it is helpful to condense the tables above to a few representative numbers. We do this by averaging the performance over the field angles and colors in the tables above.

Performance of Perfect Corrector Averaged Over Field Angle and Color

Configuration	50% EE Diameter (μm)	80% EE Diameter (μm)	90% EE Diameter (μm)
Imaging	12	18	24
Spectroscopy	40	59	69

We can now construct an error budget for the imaging configuration based on the bare Cassegrain error budget:

Error Budget for Wide Field Imaging

Error Source	50% EE Dia. (arcseconds)	Equivalent r_0 (cm)	90% EE μm
Tracking and Drives	0.070	∼144	21
Secondary Alignment and Focus	0.090	∼112	28
Primary Mirror Surface	0.170	∼59	52
Primary Conic/Radius	0.075	∼135	23
Secondary Mirror Surface	0.040	∼253	12
Secondary Conic/Radius	0.028	∼361	9
Telescope Seeing (5%)	0.060	∼168	18
Best Atmospheric Seeing	0.225	∼45	68
Corrector Optical Design	0.065	∼156	20
Corrector Fabrication	0.065	∼156	20
Primary Alignment	0.036	∼280	11
Corrector Alignment	0.018	∼560	5
Best Final Image* (total)	0.338	∼30	103

*Averaged over field angle and color.

The error budget for the spectroscopic configuration:

Error Budget for Wide Field Spectroscopy

Error Source	50% EE Dia. (arcseconds)	Equivalent r_0 (cm)	90% EE μm
Tracking and Drives	0.070	∼144	21
Secondary Alignment and Focus	0.090	∼112	28
Primary Mirror Surface	0.170	∼59	52
Primary Conic/Radius	0.075	∼135	23
Secondary Mirror Surface	0.040	∼253	12
Secondary Conic/Radius	0.028	∼361	9
Telescope Seeing (5%)	0.060	∼168	18
Best Atmospheric Seeing	0.225	∼45	68
Corrector Optical Design	0.235	∼43	72
Corrector Fabrication	0.220	∼46	67
Primary Alignment	0.070	∼144	21
Corrector Alignment	0.070	∼144	21
Best Final Image* (total)	0.467	∼22	143

*Averaged over field angle and color.

5.3.4 Differential Image Distortion Specifications

Differential image distortion is most serious for wide field spectroscopic applications, where differential distortion will result in light loss at the slit or optical fiber. The pattern of distortion will in general change with time as the instrument rotates or the telescope collimation changes. We set as a limit 0.15 arcseconds for the movement of the image centroid from the mean position at the edge of the spectroscopic field due to differential distortion. This corresponds to 0.30 arcseconds (50 μm) for the maximum differences in radial position for two points 30 arcminutes off axis. We assume that, in general, differential distortion arising from different misalignments will add in quadrature, but this assumption will fail at times.

Wide Field Differential Distortion Error Budget

Differential Distortion Source	Offset (μm)
Primary Collimation	5
Primary Mechanical/Optical Fab.	4
Secondary Collimation	1
Corrector Collimation	35
Corrector Fabrication	35
Total	50

The second table entry refers to the accuracy to which the optical axis of the primary mirror coincides with the mechanical reference surfaces on the mirror. These issues are discussed further in section 7.

5.3.5 Surface Roughness Specifications

Given the number of surfaces in the refractive corrector (ten in the spectroscopic configuration, and six in the imaging configuration) scattering losses are important. The best available antireflection coatings will produce losses of $\sim$1% per surface; if we were to allow the same 3% scattering losses produced by the reflective optics, we would be giving away close to half the light! Fortunately, scattering losses from the surface roughness of refractive surfaces are reduced by a factor of (n-1)/2 as compared with reflective surfaces. Furthermore, the optics are smaller and tighter specifications are possible at reasonable cost. If we specify 3 nm rms surface roughness at small scales (1 cm at the primary scales to 0.2 mm at the corrector), we obtain a scattering loss of $\sim$0.1% at 3500 Å.

6 Optical Fabrication and Support Tolerances

6.1 Primary Fabrication and Support Tolerances

6.1.1 Error Allocation

John Hill has proposed an error budget for the primary mirror surfaces which we adopt here. Unlike the telescope error budget discussed in section 5.2, where the errors are propagated as a RSS (root sum square) of image FWHM, John has chosen to propagate the structure functions. In this case, neglecting scattering:

$$\delta^2(x) \propto r_0^{5/3} \tag{8}$$

and we must propagate errors as $\Sigma r_0^{-1.67}$. In this case, the RSS of the image FWHM will not yield the same answer.

Error Source	Image FWHM at zenith (arcsec)	$\mathbf{r_0}$ at zenith (cm)	Image FWHM at 30° elevation (arcsec)	$\mathbf{r_0}$ at 30° elevation (cm)
Polishing/Testing	0.093	109	0.093	109
Primary Support[1]	0.072	141	0.130	78
Wind Forces	0.050	214	0.083	122
Ventilation Errors	0.050	214	0.050	214
Material Homogeneity	0.050	214	0.050	214
Reflective Coating	0.025	400	0.025	400
Total Primary	0.170[2]	60	0.220[2]	45

[1] Includes design and operation
[2] r_0 error propagation

6.1.2 Primary Figure Errors–Bare Cassegrain

John Hill suggests that we allow a 0.056 arcsecond FWHM (50% encircled energy diameter = 0.056 arcseconds, r_0 = 180 cm) term for primary mirror aspheric errors. If we keep the focal plane position fixed, we find that varying the primary conic by ±0.0001 or the primary radius of curvature by ±8 mm uses this entire error budget. If we allow the focal surface to shift, we find that very substantial conic errors can be accommodated with a negligible loss of image quality. Each 0.00025 change in the primary conic shifts the focal plane by ∼10 mm, and the position of the secondary by ∼0.5 mm.

Similarly, changes in the primary radius of curvature can be accommodated with a negligible loss of image quality if the focal surface can be shifted. Each 20 mm change in the primary radius of curvature shifts the focal plane position by 10 mm and the secondary position by 10 mm. However, the corrected f/5 foci are less tolerant of errors in the primary radius and conic.

6.1.3 Primary Figure Errors–Wide Field

The Run 121796AV and Run 121896AR corrector/secondary prescriptions have been changed to allow at least 10 mm of shim space between the corrector cell and its mounting surface and the f/5 instruments and the instrument rotator. These shims allow us to correct the spherical aberration introduced by small errors in the primary conic. Beginning with version 6 of these specifications we allow a ± 0.00025 error in the primary conic rather than the originally specified ± 0.0001. This change accomodates the maximum expected error due to primary metrology.

We have introduced corrective shims because we wish to complete fabrication of the corrector before the primary and secondaries are tested in the telescope to avoid excessive delays. The precise primary conic will not be known until some time after the converted telescope is assembled.

The lateral color is unaffected by small changes in the primary figure.

Primary Conic -1.00025 (-0.00025 from Nominal)
Imaging Configuration–Run 121896AR
Corrector and Focal Plane Shifted ∼+10 mm

Diameter to Encircle 90% of the Energy (in μm)

Field Angle	3300Å	3500Å	4000Å	4775Å	6772Å	10000Å
$0'$	21	12	10	16	21	23
$8.75'$	42	35	22	17	15	18
$14'$	42	33	22	20	23	30
$17.5'$	28	27	23	22	22	29

Primary Conic -0.99975 (+0.00025 from Nominal)
Imaging Configuration–Run 121896AR
Corrector and Focal Plane Shifted ∼-10 mm

Diameter to Encircle 90% of the Energy (in μm)

Field Angle	3300Å	3500Å	4000Å	4775Å	6772Å	10000Å
$0'$	23	14	10	15	20	22
$8.87'$	37	30	18	13	14	17
$14'$	34	26	19	23	28	35
$17.5'$	25	25	25	25	30	39

The 90% encircled energy diameter averaged over field angle and color is 24 μm for a primary conic of -1.00025 and 23 μm for a primary conic of -0.99975. If we compare these numbers to the 24 μm contributed by the "perfect" corrector, we find that there is no loss of image quality, and the limit is set by the shim allowance in the instrument and corrector mounting (now 10 mm).

Primary Radius -16236 mm (+20 mm from Nominal)
Imaging Configuration–Run 121896AR
Corrector and Focal Plane Shifted ∼+10 mm

Diameter to Encircle 90% of the Energy (in μm)

Field Angle	3300Å	3500Å	4000Å	4775Å	6772Å	10000Å
$0'$	22	13	10	15	21	23
$8.87'$	41	31	20	15	15	16
$14'$	38	30	19	19	25	32
$17.5'$	27	25	23	23	25	34

Primary Radius -16276 mm (-20 mm from Nominal)
Imaging Configuration–Run 121896AR
Corrector and Focal Plane Shifted ∼-10 mm

Diameter to Encircle 90% of the Energy (in μm)

Field Angle	3300Å	3500Å	4000Å	4775Å	6772Å	10000Å
$0'$	22	13	10	15	21	23
$8.87'$	41	31	20	15	15	16
$14'$	38	30	19	19	25	32
$17.5'$	27	25	23	23	25	34

The 90% encircled energy diameter averaged over field angle and color is 23 μm for a primary radius of -16236 mm and 23 μm for a primary radius of -16276 mm. Here again the limit is set by the shim allowance rather than the image quality. Because the primary conic is harder to measure than the primary radius, we set a tighter spec on the primary conic.

6.1.4 Summary of Primary Figure Error Budget

The spectroscopic corrector configuration behaves in the same fashion as the imaging configuration. We find that the currrent allowance of ± 0.00025 in the conic and ± 2.5 mm in the radius will be satisfactory.

6.2 Secondary Fabrication and Support Tolerances

6.2.1 Error Allocation

The secondary error budget is constructed in a similar fashion except that the pupil size is considerably smaller at the secondary mirrors. The pupil demagnifications at the various secondaries (for the bare Cassegrain systems) are shown in the table below.

Secondary	Pupil Demagnification
f/5	4.13
f/9	6.69
f/15	9.93

The performance of the secondary, which we have specified as $r_0 = 253$ cm, can then be scaled to wavefront errors at the secondary by the factors in the table above. For example, at f/5 we must achieve $r_0 = 61$ cm, as measured at the secondary. This is very close to the primary specification, so the physical wavefront errors at the secondary expressed in r_0 can be the same as for the primary. However, the scaling to image FWHM will be much more favorable.

The specifications for the f/9 secondary are also shown. They were derived by modifying the f/5 specifications by the ratio of the beam demagnifications between the two secondaries. The effect produces identical contributions to the image size. See West (1997) for the detailed polishing specifications for the f/9 mirror.

Secondary Error Budget

Error Source	Image FWHM (arcsec)	$\mathbf{r_0}$ f/5 (cm)	$\mathbf{r_0}$ f/9 (cm)
Polishing/Testing	0.022	109	69
Secondary Support[1]	0.017	141	89
Wind Forces	0.011	214	135
Ventilation Errors	0.011	214	135
Material Homogeneity	0.011	214	135
Reflective Coating	0.006	400	253
Total Secondary	0.040[2]	60	38

[1] Includes design and operation

[2] r_0 error propagation

6.2.2 Secondary Figure Errors–Bare Cassegrain

We can establish the specifications for the bare Cassegrain foci to use the entire 0.028 arcsecond 50% encircled energy diameter.

Errors that Degrade the 50% EE Diameter to 0.028″

Secondary	Conic Error	Radius Error
f/5	0.0005	1.0 mm
f/9	0.0005	1.6 mm
f/15	0.0007	2.5 mm

We note that the wide field focus sets more stringent requirements for the f/5 focus (see below). The f/9 and f/15 specifications can be set by dividing the conic and radius errors by $\sqrt{2}$ to allocate equal portions to conic and radius errors. We defer the secondary figure error budget to section 6.2.4 below.

6.2.3 Secondary Figure Errors–Wide Field

Here, we assume that the primary conic error budget has used up the entire shim allowance. We therefore do not allow additional shifts of the corrector and focal surface to compensate for secondary conic errors. The lateral color is unaffected by small changes in the secondary figure.

Secondary Conic -2.697825 (-0.001 from Nominal)
Imaging Configuration–Run 121896AR

Diameter to Encircle 90% of the Energy (in μm)

Field Angle	3300Å	3500Å	4000Å	4775Å	6772Å	10000Å
$0'$	35	28	16	20	21	21
$8.87'$	55	47	31	22	19	19
$14'$	47	42	32	31	36	39
$17.5'$	38	35	32	28	28	34

Secondary Conic -2.695825 (+0.001 from Nominal)
Imaging Configuration–Run 121896AR

Diameter to Encircle 90% of the Energy (in μm)

Field Angle	3300Å	3500Å	4000Å	4775Å	6772Å	10000Å
$0'$	17	15	14	21	30	33
$8.87'$	35	30	24	21	23	27
$14'$	33	29	25	24	29	36
$17.5'$	26	23	23	26	31	38

The 90% encircled energy diameter averaged over field angle and color is 27 μm for a secondary conic of -2.695825 and 32 μm for a secondary conic of -2.697825. If we remove the 24 μm contributed by the "perfect" corrector, we find a maximum contribution of 21 μm from a secondary conic error of ± 0.001, or 0.124 arcseconds. The secondary conic/radius error budget is 0.051 arcseconds (90% EE), so we conclude that a conic error of 0.0004 would use the entire error budget. If we allocate equal portions to the conic and radius errors, we arrive at a budget of 0.0003 for the conic error.

Secondary Radius -5153.074 mm (-2.1 mm from Nominal)
Imaging Configuration–Run 121896AR

Diameter to Encircle 90% of the Energy (in μm)

Field Angle	3300Å	3500Å	4000Å	4775Å	6772Å	10000Å
$0'$	17	15	14	21	30	33
$8.87'$	35	29	24	21	23	26
$14'$	33	29	25	24	29	36
$17.5'$	26	24	23	26	31	37

Secondary Radius -5148.874 mm (+2.1 mm from Nominal)
Imaging Configuration–Run 121896AR

Diameter to Encircle 90% of the Energy (in μm)

Field Angle	3300Å	3500Å	4000Å	4775Å	6772Å	10000Å
$0'$	34	28	16	20	21	21
$8.87'$	55	44	31	22	19	19
$14'$	47	42	32	31	36	39
$17.5'$	38	35	31	28	28	34

The 90% encircled energy diameter averaged over field angle and color is 31 μm for a secondary radius of -5148.874 mm and 26 μm for a secondary radius of -5153.074 mm. If we remove the 24 μm contributed by the "perfect" corrector, we find a maximum contribution of 20 μm from the radius error, or 0.118 arcseconds. The secondary conic/radius error budget is 0.051 arcseconds (90% EE), so we conclude that a radius error of 0.91 mm would use the entire error budget. If we allocate equal portions to the conic and radius errors, we arrive at a budget of 0.64 mm for the radius error.

6.2.4 Summary of the Secondary Figure Error Budget

The error budget for the f/5 secondary is driven by the wide field focus; we summarize the error budgets in the table below.

Secondary Figure Error Budget

Secondary	Conic Error	Radius Error
f/5	0.0003	0.6 mm
f/9	0.0004	1.1 mm
f/15	0.0005	1.8 mm

6.3 Corrector Fabrication Tolerances

The following section is a summary of the specifications given in "Fabrication Specifications for the SAO Wide-Field Corrector Elements", Fabricant (1995).

6.3.1 Encircled Energy and Lateral Color Specifications

The error budget requires a contribution to the 90% encircled energy of less than 20μm (imaging) and 67μm (spectroscopy) from fabrication errors in the corrector. This can be met by requiring that the 90% encircled energy diameters (predicted by ZEMAX-EE from measurements of the as-fabricated elements) are no more than 10% (or 8μm, whichever is greater) larger than the values tabulated for the perfect corrector (section 5.3.2). In addition, the maximum lateral color at the 50%, 80% and full field angles (predicted by ZEMAX-EE from measurements of the as-fabricated elements) must be no more than 5 μm larger than the values tabulated in Section 5. These specifications for encircled energy and lateral color must be held for both the Run 121896AR and Run 121796AV configurations. We summarize these specifications for both configurations below.

Manufacturing Specifications for Run 121796AV Optics
Diameter to Encircle 90% of the Energy (in μm)

Field Angle	3300$\mathring{A}$	3500$\mathring{A}$	4000$\mathring{A}$	4775$\mathring{A}$	6772$\mathring{A}$	10000$\mathring{A}$
$0'$	57	50	38	29	23	24
$15'$	63	66	72	77	82	87
$24'$	72	72	75	77	82	87
$30'$	132	127	119	116	118	123

Manufacturing Specifications for Run 121896AR Optics
Diameter to Encircle 90% of the Energy (in μm)

Field Angle	3300$\mathring{A}$	3500$\mathring{A}$	4000$\mathring{A}$	4775$\mathring{A}$	6772$\mathring{A}$	10000$\mathring{A}$
$0'$	31	23	17	23	28	30
$8.87'$	49	40	27	22	21	24
$14'$	49	39	28	28	33	40
$17.5'$	36	34	33	31	33	41

Run 121796AV Lateral Color Specifications
Maximum Image Centroid Spread Between 3300 and 10000 $\AA$

Field Angle	Shift (μm)
$0'$	5
$15'$	61
$24'$	34
$30'$	42

Run 121896AR Lateral Color Specifications
Maximum Image Centroid Spread Between 3300 and 10000 $\AA$

Field Angle	Shift (μm)
$0'$	5
$8.87'$	21
$14'$	12
$17.5'$	27

These specifications give 90% encircled energy diameters, averaged over field angle and color, of 78 μm and 32 μm respectively. If we remove the 69 μm and 24 μm contributed by the "perfect" corrector, we obtain fabrication errors of 36 μm and 21 μm, respectively. These correspond to 90% encircled energy diameters of 0.22 and 0.12 arcseconds, which meet the error budget.

6.3.2 Differential Image Distortion Specifications

The assembled corrector shall have less than 35 μm of differential distortion at the field edges of each of the two configurations as specified in section 5.3.4.

6.3.3 Optical Axis Offset Specifications

The assembled corrector shall have less than 50 μm of image displacement at the focal surface from the geometrical axis defined by the corrector cell, as predicted by ZEMAX. We assume for this specification that the corrector elements will be mounted into the cell by reference to their machined edges with no additional error. Note that for Run 121796AV, this specification includes the contribution of the ADC prism fabrication errors.

6.3.4 Small Scale Surface Errors and Roughness Specifications

Here, we specify the maximum allowable surface errors at scales of 5 to 40 mm. We adopt a specification based on area-weighted slope errors. The maximum distance from the optical elements to the focal plane is ∼1800 mm, so a wavefront slope error of 10^{-5} radians would cause an image blur of 18 μm at the focal surface. We require a total contribution of less than 5 μm, and so specify that the area-weighted slope errors on the element surfaces on scales of 5 to 40 mm be less than 5×10^{-6} radians.

The elements shall have a 20 Å RMS surface roughness at spatial scales smaller than 5 mm.

The elements shall be finished to a Mil 60/40 scratch-dig specification in the optical clear aperture.

7 Collimation Tolerances

7.1 Introduction

For most purposes we will define the axis of the instrument rotator as the fundamental axis of the telescope. This is a useful definition for several reasons. 1) The rotator axis must define the pointing axis of the telescope to avoid having tracking errors. 2) It is the easiest axis to locate because it can be determined by turning the rotator. 3) The instrument rotator axis has no active control so it provides a fixed reference.

We must then consider the effects of misalignments of the primary, secondary and corrector with respect to the rotator axis. Because the aberrations due to misalignments of the primary and the secondary are very strongly coupled to each other, we will consider the following more independent set of misalignments: 1) the secondary with respect to the primary/corrector/rotator, 2) the primary/secondary combination with respect to the corrector/rotator, and 3) the corrector with respect to the other three elements. We begin with a summary of the flexure of the telescope due to gravity. Then we establish the sensitivities of image quality and differential distortion due to the three modes of misalignment and construct an error budget.

7.2 SG&H Finite Element Predictions

As part of the design of the optics support structure (OSS) and cell of the converted MMT, Simpson, Gumpertz and Heger (SG&H) created a finite element model of the telescope. These finite element models predict deflections of the secondaries, focal point in the instrument and corrector mounting flange with respect to the mounting locations of the primary hardpoints in the primary cell. These deflections should probably be interpreted as lower limits since realistic secondary and primary supports and instrument rotators must be added to the structural deflections from the finite element model.

These results were culled from the three J. Antebi memos listed in the references. The deflections have been calculated for gravity loads with the telescope zenith and horizon pointing, as well as for wind loads of 17 meters/second (40 mph) with the telescope zenith pointing and at an elevation of 45°. In each case, a 1360 kg instrument load located 2.77 m behind the primary mirror vertex was applied. The deflections are tabulated at the secondary vertices and at the (on-axis) focal point in the instrument.

In the following, the coordinate system is fixed with respect to the primary mirror and rotates with the primary. The X axis runs parallel to the elevation axis, the Y axis points upwards when the telescope is horizon pointing and Z runs parallel to the optical axis of the primary. The linear deflections are in μm, the rotations are in

arcseconds.

F/5 Secondary

Element	Deflection	Gravity Horizon	Gravity Zenith	Wind Zenith	Wind Elevation=45°
Secondary	Δ Y	-774	-119	39	46
Secondary	Δ Z	-14	-469	-0.81	-0.96
Secondary	$\Delta\theta_X$	-4.92	3.24	-1.75	-1.71
Corrector	Δ Y	44	-40		
Corrector	Δ Z	-25	-165		
Corrector	$\Delta\theta_X$	-17.40	6.48		
Instrument	Δ Y	-93	4.2	-1.5	-1.7
Instrument	Δ Z	-21	-156	2.5	2.9
Instrument	$\Delta\theta_X$	-7.18	3.85	-1.10	-1.29

F/9 Secondary

Element	Deflection	Gravity Horizon	Gravity Zenith	Wind Zenith	Wind Elevation=45°
Secondary	Δ Y	-698	-129	46	53
Secondary	Δ Z	-14	-390	-0.86	-1.02
Secondary	$\Delta\theta_X$	10.91	3.20	-1.23	-1.22
Instrument	Δ Y	-93	4.1	-1.5	-1.7
Instrument	Δ Z	-21	-156	2.5	2.9
Instrument	$\Delta\theta_X$	-7.19	3.86	-1.10	-1.29

F/15 Secondary

Element	Deflection	Gravity Horizon	Gravity Zenith	Wind Zenith	Wind Elevation=45°
Secondary	Δ Y	-684	-136	43	51
Secondary	Δ Z	-14	-175	-0.81	-0.96
Secondary	$\Delta\theta_X$	17.87	2.89	-1.20	-1.34
Instrument	Δ Y	-93	4.1	-1.4	-1.6
Instrument	Δ Z	-20	-156	2.3	2.7
Instrument	$\Delta\theta_X$	-7.56	3.86	-1.04	-1.22

7.3 Instrument Rotator Tolerances

J.T. Williams has summarized the goals for the rotator performance; we restate those goals relevant to the optical performance here. Some of the original goals from J.T.'s 1992 memo have been altered.

- The maximum slew speed of the rotator will be 2° per second; the maximum tracking speed will be 1.3° per second.
- The tracking performance of the rotator will add no more than 0.1 arcsecond (17 μm) FWHM to the image diameter at the edge of the 1° (6348 mm) diameter field.
- Tracking resolution corresponds to 8 μm at the edge of the 1° diameter field, or an angular resolution of 0.5 arcseconds.
- The rotation accuracy goal corresponds to 85 μm at the edge of the 1° diameter field or an angular accuracy of 5 arcseconds. Rotational offsets as large as 10° can be made to an angular accuracy of 1 arcsecond, with a repeatability of 0.5 arcseconds.

We propose tightening the original specification for the decentration of the rotator axis (as the telescope elevation changes or the instrument rotates) by a factor of two to 50 μm. We also propose tightening the original specification for the maximum differential defocus due to rotator tilt at the field edges by the same factor of two to 50 μm, and the maximum axial displacement to 50 μm.

The rotator defocus as a function of elevation will be removed by focussing the secondary.

Differential defocus across the wide field will be introduced by tilts of the instrument rotator with respect to the primary mirror. The major terms arise from the compliance of the rotator bearing and the deformations of the cell. The rotator bearing will introduce less than 50 μm of differential defocus across the rotator flange diameter of $\sim$1830 mm, corresponding to a tilt of 5.6 arcseconds. The SG&H finite element results show that a maximum tilt of 11 arcseconds is introduced by the cell moving from zenith to horizon, giving a total tilt of $\sim$17 arcseconds. If we choose a compromise focus, the maximum defocus at the field edges (field radius is 305 mm) is 25 μm. This corresponds to a maximum image spread at the field edges of $\sim$4.6 μm, or 0.027 arcseconds, which may be neglected.

7.4 Secondary Collimation Tolerances

7.4.1 Secondary Collimation–Bare Cassegrain

Our error budget allows a 112 cm r_0 wavefront from decollimation, corresponding to a 50% encircled energy diameter of 0.09 acseconds. (Image FWHM are difficult to extract from ray trace codes, so we use the 50% encircled energy criterion instead; these are equivalent for a Gaussian image). We first derive sensitivities due to defocus, tilt, and decentration for each of the three secondaries. The 0.090 arcsecond specification corresponds to linear dimensions of 15 μm, 26 μm and 42 μm at f/5, f/9 and f/15, respectively. The table below gives the decollimation sensitivities. The numbers in parentheses in the table give the image displacements at the focal surface in μm.

Secondary Collimation Error
For 0.09 Arcsecond 50% EE Diameter

Secondary	Tilt Limit (arcsec)	Decenter Limit (μm)	Defocus Limit (μm)
f/5	8.3 (632)	76 (231)	6 (0)
f/9	12.6 (1040)	74 (434)	6 (0)
f/15	18.0 (1639)	71 (730)	6 (0)

We must also calculate sensitivities to focal plane tilts and decenters. For the small field, bare Cassegrain applications, focal plane tilts can be safely neglected. Focal plane decenters will be compensated by moving the telescope mount to restore the image position, so they are equivalent to operating the telescope off axis. By assigning an equal fraction of the alignment error budget to each of the error terms for the secondary, we arrive at the error budget below.

Bare Cassegrain
Secondary Collimation Error Budget

Secondary	Tilt Limit (arcsec)	Decenter Limit (μm)	Defocus Limit (μm)
f/5	4.8 (365)	44 (133)	3.5 (0)
f/9	7.3 (600)	43 (250)	3.5 (0)
f/15	10.4 (946)	41 (421)	3.5 (0)

The finite element model predicts deflections of the secondary an order of magnitude larger, therefore active control of the secondary collimation is required.

7.4.2 Secondary Collimation Sensitivities–Wide Field

Differential distortion due to secondary miscollimation is negligible (<1μm in all cases below). Therefore, the tolerances can be set by image quality alone.

8.3 Arcsec Tilt of Secondary

Spectroscopic Configuration–Run 121796AV

Diameter to Encircle 90% of the Energy (in μm)

Field Angle	3300Å	3500Å	4000Å	4775Å	6772Å	10000Å
0′	64	58	45	37	33	36
15′	67	67	68	70	72	74
24′	67	65	63	62	61	62
30′	138	130	118	109	97	98
-15′	61	65	71	79	88	92
-24′	72	75	81	85	95	101
-30′	116	113	112	116	123	133

8.3 Arcsec Tilt of Secondary

Imaging Configuration–Run 121896AR

Diameter to Encircle 90% of the Energy (in μm)

Field Angle	3300Å	3500Å	4000Å	4775Å	6772Å	10000Å
0′	38	34	35	39	44	45
8.87′	64	55	42	39	34	31
14′	62	51	41	31	26	28
17.5′	62	57	46	36	23	19
-8.87′	43	38	31	30	35	39
-14′	46	42	38	42	51	58
-17.5′	26	29	35	42	51	62

76 μm Decenter of Secondary

Spectroscopic Configuration–Run 121796AV

Diameter to Encircle 90% of the Energy (in μm)

Field Angle	3300Å	3500Å	4000Å	4775Å	6772Å	10000Å
$0'$	63	55	44	35	30	33
$15'$	61	64	71	79	86	92
$24'$	69	72	77	83	90	96
$30'$	121	118	114	114	118	124
$-15'$	65	65	66	69	70	74
$-24'$	64	63	61	61	61	65
$-30'$	125	121	110	103	93	95

76 μm Decenter of Secondary

Imaging Configuration–Run 121896AR

Diameter to Encircle 90% of the Energy (in μm)

Field Angle	3300Å	3500Å	4000Å	4775Å	6772Å	10000Å
$0'$	37	32	32	36	41	42
$8.87'$	40	33	25	26	31	35
$14'$	40	35	33	36	44	52
$17.5'$	27	30	34	40	48	56
$-8.87'$	62	56	40	35	31	28
$-14'$	61	51	42	33	30	30
$-17.5'$	53	49	41	27	18	20

6 μm Defocus of Secondary

Spectroscopic Configuration–Run 121796AV

Diameter to Encircle 90% of the Energy (in μm)

Field Angle	3300Å	3500Å	4000Å	4775Å	6772Å	10000Å
$0'$	33	24	23	25	30	35
$15'$	71	74	80	85	91	96
$24'$	75	78	79	80	83	87
$30'$	131	126	118	113	108	109

A negligible scale change is introduced by the defocus, corresponding to a 0.4 μm shift $30'$ off-axis.

6 μm Defocus of Secondary

Imaging Configuration–Run 121896AR

Diameter to Encircle 90% of the Energy (in μm)

Field Angle	3300Å	3500Å	4000Å	4775Å	6772Å	10000Å
$0'$	45	36	22	12	12	13
$8.87'$	59	51	38	28	28	30
$14'$	60	51	39	39	43	51
$17.5'$	30	21	19	26	36	48

A negligible scale change is introduced by the axial shift, corresponding to a 0.1 μm shift $15'$ off-axis.

7.4.3 Secondary Collimation Error Budget–Wide Field

Our image quality error budget for decollimation is 0.090 arcseconds FWHM or 0.164 arcseconds 90% encircled energy diameter. This corresponds to a linear dimension of 28 μm. We begin by summarizing the sensitivities to decollimation, averaging over field angle and color. We have removed the effect of the "perfect" corrector in quadrature.

	90% Encircled Energy Diameter (μm)	
Collimation Error	Spectroscopy	Imaging
8.3″ tilt	35	33
76 μm decenter	29	29
6 μm defocus	35	25

We now derive a secondary collimation error budget based on image quality alone. We allow equal contributions from each error source (16 μm).

Wide Field Secondary Collimation Error Budget

Collimation Error	Error Budget
tilt	3.8″
decenter	42 μm
defocus	2.7 μm

7.5 Telescope Axis Alignment Tolerances

Here we specify the allowable decenter and tilt of the primary/secondary mirror combination with respect to the corrector/instrument rotator. At the bare Cassegrain foci, a decenter will result only in a shift of the optical axis, which can be corrected by repointing the telescope, so we need be concerned only with the interaction with the wide-field corrector. A tilt of the primary results in a tilt of the focal plane. Therefore, the physically large focal plane of the wide-field also drives the specification.

7.5.1 Sensitivities

The sensitivities to tilt (applied at the vertex of the primary) and decenter of the telescope with respect to the corrector and rotator are as follows:

0.1° Tilt of Telescope About Primary Vertex

Spectroscopic Configuration–Run 121796AV
Diameter to Encircle 90% of the Energy (in μm)

Field Angle	3300Å	3500Å	4000Å	4775Å	6772Å	10000Å
$0'$	53	47	34	22	16	19
$15'$	72	77	82	88	91	95
$24'$	103	100	97	96	96	95
$30'$	208	200	187	175	163	155
$-15'$	65	64	71	73	75	77
$-24'$	111	113	125	132	145	158
$-30'$	103	118	132	149	173	190

The differential distortion is 45μm at $30'$. The average image degradation is 68μm.

Imaging Configuration–Run 121896AR

Field Angle	3300Å	3500Å	4000Å	4775Å	6772Å	10000Å
$0'$	26	17	13	19	24	26
$8.87'$	20	19	22	23	28	30
$14'$	40	40	40	39	40	41
$17.5'$	82	81	79	78	77	74
$-8.87'$	69	60	49	42	40	40
$-14'$	90	84	74	70	73	81
$-17.5'$	76	72	66	69	82	86

The differential distortion is 15μm at $17.5'$. The average image degradation is 42μm.

2.0 mm Decenter of Telescope
Spectroscopic Configuration–Run 121796AV
Diameter to Encircle 90% of the Energy (in μm)

Field Angle	3300Å	3500Å	4000Å	4775Å	6772Å	10000Å
$0'$	54	48	36	26	21	23
$15'$	47	49	54	59	65	72
$24'$	70	73	84	88	98	107
$30'$	97	98	111	120	143	160
$-15'$	73	75	79	83	87	91
$-24'$	83	82	83	83	83	85
$-30'$	157	149	135	128	119	115

The differential distortion is 7μm at $30'$. The average image degradation is 39μm.

Imaging Configuration–Run 121896AR

Field Angle	3300Å	3500Å	4000Å	4775Å	6772Å	10000Å
$0'$	30	22	21	25	31	33
$8.87'$	48	43	31	28	29	33
$14'$	54	49	47	47	52	60
$17.5'$	33	34	34	40	53	65
$-8.87'$	43	33	28	28	25	22
$-14'$	35	32	30	26	20	17
$-17.5'$	56	54	49	43	37	34

The differential distortion is 2.4μm at $17.5'$. The average image degradation is 27μm.

7.5.2 Error Budget

The expected deviations of the optical axis of the primary from the geometric axis of the machined surfaces of the primary mirror are 1 mm in translation and $12''$ in tilt. We assume that these differences between the geometrical and optical surfaces dominate the error budget.

The image quality error budgets for primary alignment (see section 5.3.3) are 21μm and 11μm in spectroscopic and imaging modes, respectively. The differential distortion error budget is 4μm in both modes (see section 5.3.4). The error budgets are met in spectroscopic mode. In imaging mode we expect 13.5μm of image degradation (which slightly exceeds the error budget) and negligible amounts of differential distortion.

If the offset of the primary axis is as large as 1 mm, a test to determine the exact location of the optical center of the mirror should be considered.

7.6 Primary Collimation Tolerances

Wind forces, among others, will cause the primary to move on its mount because the hardpoints are not infinitely stiff. To the extent that these motions are not corrected by the mount or other active system, these motions will degrade the image quality through image wander and through decollimation. However, as discussed in Section 8, the image wander dominates. The effects of primary collimation errors on image quality are easily derived from the secondary collimation tolerances in Section 7.4, noting that: (1) a primary decenter is equivalent to a secondary decenter and (2) a primary tilt is equivalent to a tilt and decenter of the secondary. The primary-secondary separation is given in Section 2. The wind error budget is discussed in Section 8. In our previous discussion we have assumed that the primary mirror motions are specified completely by the SG&H finite element studies, with no contribution from the hardpoints.

7.7 Corrector Collimation Tolerances

7.7.1 Corrector Deflections WRT Instrument Rotator

We use the predictions of the SG&H finite element models to predict the relative deflections of the corrector and the instrument rotator. The SG&H tables give the deflections of the corrector and the instrument focal surface with respect to the primary hardpoint mounting positions. We approximate the relative deflections of the corrector and rotator axis by subtracting the corrector and instrument deflections and adding a term for the deflection of the rotator bearing under gravity load.

Deflection	Gravity Horizon	Gravity Zenith
Corrector–Instrument		
Δ Y	137 μm	-44 μm
Δ Z	-4 μm	-9 μm
$\Delta\theta_X$	-10.2″	2.6″
Rotator Bearing		
Δ Y	-50 μm	0 μm
Δ Z	0 μm	-50 μm
$\Delta\theta_X$	-5.7″	0″
Total Corrector wrt Rotator		
Δ Y	187 μm	-44 μm
Δ Z	-4 μm	41 μm
$\Delta\theta_X^1$	-10.2″	2.6″
Decollimation[2]		
Δ Y	116 μm	
Δ Z	23 μm	
$\Delta\theta$	6.4″	

1. To be conservative, we don't assume a cancellation of rotations.
2. We can adjust the corrector position so that we experience half the total peak to peak deflection.

7.7.2 Corrector Collimation Sensitivities

We begin by describing the sensitivity of the image quality to tilts, decenters and axial movements of the optically perfect corrector.

0.01° Tilt of Corrector
About Leading Element Vertex

Spectroscopic Configuration–Run 121796AV
Diameter to Encircle 90% of the Energy (in μm)

Field Angle	3300Å	3500Å	4000Å	4775Å	6772Å	10000Å
0′	50	43	31	21	15	16
15′	59	61	66	72	76	83
24′	69	68	71	70	76	79
30′	130	124	115	110	108	113
-15′	55	57	61	65	71	76
-24′	59	60	64	70	78	84
-30′	110	108	103	102	108	124

The differential image distortion is 31 μm 30′ off-axis; the image displacement is 6 μm on-axis. No (average) scale change is introduced. The image degradation is 11μm.

0.01° Tilt of Corrector
About Leading Element Vertex

Imaging Configuration–Run 121896AR
Diameter to Encircle 90% of the Energy (in μm)

Field Angle	3300Å	3500Å	4000Å	4775Å	6772Å	10000Å
0′	23	15	10	15	20	22
8.87′	37	28	14	10	12	14
14′	34	24	14	13	20	27
17.5′	32	31	30	29	28	32
-8.87′	46	38	23	17	16	19
-14′	45	38	27	27	33	37
-17.5′	23	21	20	19	27	37

The differential image distortion is 10 μm 17.5′ off-axis; the image displacement is 2 μm on-axis. No (average) scale change is introduced. The image degradation is negligible.

0.2 mm Decenter of Corrector

Spectroscopic Configuration–Run 121796AV

Diameter to Encircle 90% of the Energy (in μm)

Field Angle	3300Å	3500Å	4000Å	4775Å	6772Å	10000Å
$0'$	51	44	30	21	15	16
$15'$	56	58	63	68	75	79
$24'$	63	63	66	69	75	79
$30'$	118	113	107	104	106	114
$-15'$	57	59	65	69	75	79
$-24'$	65	65	67	69	73	79
$-30'$	122	117	109	105	107	113

The differential image distortion is 26 μm $30'$ off-axis; the image displacement is 7 μm on-axis. No (average) scale change is introduced. The image degradation is negligible.

0.2 mm Decenter of Corrector

Imaging Configuration–Run 121896AR

Diameter to Encircle 90% of the Energy (in μm)

Field Angle	3300Å	3500Å	4000Å	4775Å	6772Å	10000Å
$0'$	24	15	10	16	20	22
$8.87'$	38	31	18	13	14	16
$14'$	38	29	20	21	27	33
$17.5'$	27	25	24	23	26	35
$-8.87'$	42	33	19	15	14	15
$-14'$	42	32	21	17	24	31
$-17.5'$	29	27	24	23	24	32

The differential image distortion is 8 μm $17.5'$ off-axis; the image displacement is 4 μm on-axis. No (average) scale change is introduced. The image degradation is negligible.

1.0 mm Axial Shift of Corrector

Spectroscopic Configuration–Run 121796AV

Diameter to Encircle 90% of the Energy (in μm)

Field Angle	3300Å	3500Å	4000Å	4775Å	6772Å	10000Å
$0'$	52	44	32	23	12	15
$15'$	56	58	63	68	74	79
$24'$	67	66	69	69	74	78
$30'$	130	124	115	109	108	113

A small scale change is introduced by the axial shift, corresponding to a 18 μm shift $30'$ off-axis. About 17μm of image degradation is introduced.

1.0 mm Axial Shift of Corrector

Imaging Configuration–Run 121896AR

Diameter to Encircle 90% of the Energy (in μm)

Field Angle	3300Å	3500Å	4000Å	4775Å	6772Å	10000Å
$0'$	20	12	12	17	22	24
$8.87'$	40	31	19	14	13	16
$14'$	40	32	21	20	26	33
$17.5'$	23	25	23	22	25	34

A very small scale change is introduced by the axial shift, corresponding to a 3 μm shift $17.5'$ off-axis. A negligible amount of image degradation is introduced.

7.7.3 Corrector Collimation Error Budget

Referring to sections 5.3.3 and 5.3.4 we recall that our error budget for image degradation due to corrector alignment is 5μm in the imaging mode and 21μm in the spectroscopic mode. We allow 35μm of differential distortion.

Flexure The corrector collimation errors described above in section 7.7.1 (0.01° tilt, 0.2 mm decenter, and 1.0 mm axial shift) have a relatively small effect on the image quality. The tilt and decenter degrade the images on one side of the axis, but improve the images on the opposite side. When we average over field angle and color, there is only a small change in the image quality. However, we must be concerned with the differential distortion introduced by corrector miscollimation. We summarize the effects of the collimation errors in the table below. The differential distortion is tabulated for the spectroscopic configuration which is much larger than for the imaging configuration. The scale change introduced by the 44 μm axial shift is less than 1 μm at the edge of the spectroscopy field, and may be neglected.

Corrector Flexure Error Budget

Error Source	Error Magnitude	Differential Distortion	90% Energy Imaging	90% Energy Spectroscopy
Δ Y	116 μm	15 μm	0μm	4μm
$\Delta\ \theta$	6.4″	6 μm	0μm	2μm

These differential distortions will add, so we acquire a maximum of 21 μm of differential distortion.

Initial Alignment The total differential distortion error budget for corrector alignment is 35μm, so if we remove in quadrature the 21μm expected from flexure, we are left with 28μm for the initial alignment of the corrector. Dividing this equally between translation and tilt we can allow 150μm of translation and 23″ of tilt.

If we allow the initial axial positioning of the corrector to be good to 1 mm, we introduce 17μm of image degradation in spectroscopic mode and a negligible amount in imaging mode. The total image quality degradation from corrector flexure and initial alignment error is negligible in imaging mode and 18μm in spectroscopic mode, so the error budget in section 5.3.3 is met.

7.8 Secondary Actuator Range and Resolution

We assume that the secondary will be actuated using a hexapod, i.e. that tilt, translation, and focus are all controlled by the same actuators. For all three secondaries, the resolution is dictated by the focus specification. For all three secondaries, the focus tolerance is 3μm. Thus, we suggest a focus resolution of 3μm or smaller.

The focus range required by temperature changes is 3 mm over a 50°C temperature range. Flexure of the secondaries relative to the primary are roughly 0.7mm in translation and 0.5mm in focus. Additionally the primary mirror axis may be displaced by as much as 1.5mm from the mechanical center of the telescope at the location of the secondary. We recommend at least 10mm full range of the secondary focus motion, which will cover temperature and flexure and will also allow some latitude in the location of instruments at the focal plane. The roughly 5mm of extra motion corresponds to a freedom in the focal plane location of 90mm, 215mm, and 460mm at f/5, f/9 and f/15, respectively. (See section 7.5.2)

7.9 Primary Hardpoints

7.9.1 Introduction

The primary mirror is located in its cell with a Stewart platform parallel manipulator (Stewart 1965), which we call the hardpoint platform. The platform can be described as two planes (the cell backplate and the mirror backplate) whose orientation with respect to each other is controlled with 6 adjustable struts (hardpoints) containing flexures near each attachment. The hardpoints are grouped into 3 pairs with a near-common connection at the cell backplate and separate connections at the mirror backplate.

The platform provides precise positioning of the mirror within the cell, constrains the six degrees of solid body motion of the mirror, and provides stiffness to the support system to oppose gravity and wind loading. However, the weight of the mirror is not supported by the hardpoints–rather by 104 axial and 54 lateral pneumatic actuators. The forces on these actuators are derived in three parts: 1) the force distribution calculated from FE models that maintains surface figure under ideal theoretical conditions (see BCV reports No. 1 1989, No. 4 1991, No. 6, 1994, and No. 7 1994), 2) real-world optimization of these forces, and 3) the removal of rigid-body forces and moments acting upon the mirror through a transformation that nulls the forces on the six hardpoints (the outer-loop servo).

The mirror is protected from large forces in the event of a support failure as well as from torques acting about the hardpoint connections. This protection is provided by incorporating high-force tension and compression breakaways into the hardpoint design. In the event that the hardpoints break away, the primary comes to rest on the static supports. Since the weight of the hardpoints would otherwise put unwanted moments into the mirror connection, each hardpoint has its own counterweight system that counteracts gravity.

The the hardpoints are motorized and encoded to allow for remote control of their lengths. This provides for solid-body motion of the primary mirror, which is to be used for: (1) optical and mechanical alignments, (2) moving the mirror onto and off of the static supports and (3) to optionally compensate for cell deflection for the wide-field imaging and spectroscopic modes).

Below we describe the force, positioning, counterweighting, and stiffness specifications for the hardpoints required to meet the optical specifications of the telescope.

7.9.2 Hardpoint Geometry, Stiffness, Forces, and Torques

Force-Torque Matrix The six forces observed on the hardpoints ($f_{1...6}$) can be converted to the solid-body forces and torques acting on the mirror ($F_{x,y,z}, T_{x,y,z}$). The solid body forces are given by the projections (direction cosines) of the hardpoint vectors onto each axis which are given by vector dot products:

$$F_x = \sum_{i=1}^{6} f_i \frac{(\vec{hp_i} \cdot \hat{x})}{|\vec{hp_i}|} = \sum_{i=1}^{6} f_i (\hat{hp_i} \cdot \hat{x})$$

where $\hat{x}$ is the unit vector along the x-axis, and $\hat{hp_i}$ is a unit vector oriented along each hardpoint axis. Similar equations follow for the y and z-axes.

The solid-body mirror torque about the x-axis is given by:

$$T_x = \sum_{i=1}^{6} f_i (\hat{x} \cdot (\vec{r_i} \times \hat{hp_i}))$$

where $\vec{r_i}$ is a vector from the origin (vertex) to the upper workpoint. The upper workpoint is the intersection of the hardpoint axis with the mirror backplate midplane. Similar equations follow for the other axes. For our axisymmetric platform $|\vec{r_i}|$=2321.2 mm.

For the MMT hardpoint geometry we obtain (see West 1996b and West et al. 1996 for more information):

$$\begin{vmatrix} F_x \\ F_y \\ F_z \\ T_x \\ T_y \\ T_Z \end{vmatrix} = \begin{vmatrix} \text{-0.560} & \text{-0.433} & 0.127 & \text{-0.127} & 0.433 & 0.560 \\ \text{-0.176} & \text{-0.397} & 0.574 & 0.574 & \text{-0.397} & \text{-0.176} \\ \text{-0.809} & \text{-0.809} & \text{-0.809} & \text{-0.809} & \text{-0.809} & \text{-0.809} \\ \text{-1853.621} & 320.565 & 1533.045 & 1533.045 & 320.565 & \text{-1853.621} \\ 699.999 & 1955.204 & 1255.265 & \text{-1255.265} & \text{-1955.204} & \text{-699.999} \\ 1130.986 & \text{-1130.992} & 1130.992 & \text{-1130.992} & 1130.992 & \text{-1130.992} \end{vmatrix} \begin{vmatrix} f_1 \\ f_2 \\ f_3 \\ f_4 \\ f_5 \\ f_6 \end{vmatrix}$$

where the torques are measured in Nmm.

Stewart Platform Stiffnesses: Assuming an infinitely rigid mirror and cell, we can use the direction cosines given above to estimate the lateral and axial resonances of the Stewart platform:

$$\nu_{axial} = \frac{1}{2\pi}\sqrt{\frac{4.85 \times 10^6 K_{hp}}{m}} = 37Hz$$

and

$$\nu_{lateral} = \frac{1}{2\pi}\sqrt{\frac{2.29 \times 10^6 K_{hp}}{m}} = 25Hz$$

where K_{hp} = 95 N/μm is the measured stiffness of the hardpoint (the minimum stiffness specification was set at 80 N/μm in 1994), and m is the mass of the mirror, 8500 kg. The factors multiplying K_{hp} are the sum of the absolute values of the direction cosines from each of the six hardpoints and a conversion from m to μm. These stiffnesses are sufficient to suppress unwanted image motion due to mirror vibration in mean wind velocities exceding 10 m s^{-1} (see section 8.4). Including the mirror and cell compliances will degrade the stiffness estimates, but this calculation is beyond the scope of this section.

7.9.3 Hardpoint Stray Force Limits

Incomplete force cancellation from the counterweight and servo systems will always leave some residual forces on the hardpoints that will affect the mirror figure. The softest bending mode of the mirror is astigmatism. The sensitivity of an 8.0-m f/1.2 honeycomb mirror to this type of bending has been modeled through finite element analysis by BCV (1989) for the LBT project. BCV considered the load case with four forces at the outer permimeter of the mirror (up at the N, S positions, and down at E, W) and found that 14 N of force applied at each location produces an image blur of 0.06 arcseconds. Astigmatic forces scale as r^2t^{-3} giving a scale factor of 1.02 or 14.2 N for the 6.5 m primary (where r is the radius of the mirror and t the thickness). The FEA modelling shows that, on average, about 5x more lateral force than axial force is required to produce a given astigmatism.

We can use this result to place very rough limits on the uncompensated stray forces allowed at the hardpoint connection. Scaling 14 N of edge force to the equivalent force at the hardpoint connection radius (0.7 radius) gives 28 N. Dividing by 6 hardpoints gives 4 N axial and 20 N lateral allowable stray force.

However, a better approach is to extend the FEA results for the axial force sensitivity of the distributed air support system (BCV 1988 and Hill 1995). From this we find that to control astigmatism to the accuracy described above, the actuator forces must be accurate to ~1:1000 to control systematic effects and 1:200 for random effects (systematic effects result from actuator errors producing a spatial pattern). Since

the effect of an error in a single hardpoint is somewhere between systematic error produced by many support system actuators and a random error of a single actuator, we can set a better limit on the *uncompensated forces (near the hardpoint connection to the mirror)* as ∼1:500 of the axial force of a force actuator:

- < 2 N axial force
- < 10 N lateral force

Larger stray forces are permitted at the hardpoint connection if they are repeatable and can be sensed and removed. An estimate of these forces is difficult to provide given the complexity of the outer loop interaction between the hardpoints and actuators, and apparently no specific FEA exists on the subject. It is probably reasonable to assume such forces could be between 3-5 times the uncompensated forces.

7.9.4 Force Breakaway

One of the primary functions of the hardpoints is to provide the stiffness of the support system. They must remain stiff against changing gravity and wind loading. However, somewhere between the allowable stray and dynamic wind forces and the forces that begin to threaten the safety of the mirror, the hardpoints must break away.

Stresses in the mirror blank must not exceed 0.7 MPa (100 psi) for an extended period of time (Hill 1995).

Glass Safety – Force and Moment Limits: The hardpoints do not attach directly to the mirror, but rather through an intermediate E6 glass wedge. Scaling from recent FEA models of the E6 wedge-to-mirror connection (Cuerden 1996, Table 3), we obtain the forces (applied at the hardpoint upper flexure) that produce 100 psi stresses in the mirror blank:

Axis	Force to produce 100 psi	Equiv. moment about the backplate midplane (under wedge center)	Force detected by Hardpoint load cell
	N	Nmm	N
X′	232.6	38,500	400
Y′	267.3	54,800	detected by other hardpoints only
Z′	274.4	33,100	340
HP	1438	NA	1438
$HP_{\perp}$	180	36,700	detected by other hardpoints only

The second column gives the maximum mirror stress near the wedge attachment. The exact location of the peak stress depends on the load vector. X′, Y′, and Z′ are defined in the coordinate system of the counterweights. X′ is parallel to the hardpoint's axis projected in the xy plane, Y′ is perpendicular to this axis but parallel to the xy plane, and Z′ is parallel to the optical axis. HP is directly along the hardpoint axis and $HP_{\perp}$ is perpendicular to HP but in the plane of the hardpoint and the mirror axis. Relatively high forces are allowed for designed loading of the Stewart platform members (i.e. along HP), but much smaller loading from hardpoint counterweight malfunctions is permitted. Additionally, Ceurden (1996b) has calculated a detailed error budget for the counterweight system.

Wind Forces: The hardpoints must remain stiff under wind loading. The following table gives estimates for the expected static and dynamic wind loading of the unshielded primary mirror pointed directly into the wind (West and Martin 1995). The dynamic wind is corrected for turbulence decorrelation across the mirror surface. The forces are projected onto each hardpoint using the final geometry (West 1996b). The outer loop compensates the static drag force and a portion of the dynamic force (given by the frequency response of the servo). The hardpoint breakaway force must exceed the highest dynamic wind force detected by the hardpoint with the inner loop servo running.

The following table shows that a 1 Hz outer-loop correction removes more than half of the dynamic wind forces. As shown by the last column, the resulting load on the hardpoints is far less than the breakaway force. The values in the table correspond to the primary mirror pointed directly into the mean wind vector.

Mean wind velocity	Static wind force on mirror	Static force sensed by each hardpoint (outer loop off,on)	RMS dynamic force produced by wind (outer loop off,on)	RMS dynamic force sensed by each hardpoint (outer loop off,on)
m s^{-1}	N	N	N	N
6.7	660	136, ∼0	180, 61	38, 13
22	7050	1450, ∼0	1900, 930	390, 190

Hardpoint Force Specifications:

- Hardpoints are required to maintain the stiffness specification of 80 N/μm over the range ±300 N.
- Uncompensated stray forces of < 2 N axial and < 10 N lateral are allowed. Forces that are repeatable, detected and compensated may be 3-5x these values.
- Outer loop servo force resolution : 0.5 N over ±300 N.

- Outer loop monitor force resolution: 2 N over ±3000 N.
- Maximum breakaway force: 1440 N. The nominal pressure applied to the hardpoint breakaway pistons is 4 bar (58 psi) which produces average tension and compression breakaway forces of 1600 N and 1100 N, respectively, Tomelleri (1996). At this pressure, the tension breakaway exceeds the 100 psi mirror safety by about 10%. Although this is not a problem for transient breakaways, it could be a problem during a protracted breakaway. Reducing the piston pressure by 10-15% is advisable.
- Maximum moment allowed on hardpoint body: 3500 Nmm (limited by clearance of the vane flexure slots). The flexures are rigid for larger moments resulting in very large forces being applied to the mirror.

7.9.5 Hardpoint Positioning

In addition to providing the stiffness of the support system, the hardpoints allow the precise positioning of the primary mirror within its cell. Here we describe how to calculate the hardpoint length changes required to achieve general solid body motions of the primary mirror.

Coordinate System: The coordinate system is defined with the origin at the mirror vertex with the mirror in the nominal working position (i.e. mirror backplate is 4 mm above the static supports and laterally centered). The +Z axis is along the optic axis and points toward the secondary. The +Y axis (called the lateral axis) is along the elevation axis and points upward when the mirror is horizon pointing. The +X axis (called the cross-lateral) is oriented along the elevation bearing axis, forming a right-handed coordinate system.

Translation-Rotation Matrix: A method for determining the hardpoint length changes corresponding to solid body motions of the mirror is outlined in West (1996a) and yields the following transformation for our geometry:

$$\begin{vmatrix} \Delta l_1 \\ \Delta l_2 \\ \Delta l_3 \\ \Delta l_4 \\ \Delta l_5 \\ \Delta l_6 \end{vmatrix} = \begin{vmatrix} 560.4 & 176.4 & 809.3 & -5.5 & -3.4 & 9.0 \\ 433.0 & 397.1 & 809.3 & 5.5 & -9.5 & -1.6 \\ -127.4 & -573.5 & 809.3 & -5.5 & -6.1 & -7.4 \\ 127.4 & -573.5 & 809.3 & 5.5 & 6.1 & -7.4 \\ -432.9 & 397.2 & 809.3 & -5.5 & 9.5 & -1.6 \\ -560.3 & 176.5 & 809.3 & 5.5 & 3.4 & 9.0 \end{vmatrix} \begin{vmatrix} \Delta X \\ \Delta Y \\ \Delta Z \\ \Delta \Phi \\ \Delta \Theta \\ \Delta \Psi \end{vmatrix}$$

where Δl_i is the length change of the ith hardpoint in μm, ΔX, ΔY, and ΔZ are mirror translations in mm, and $\Delta\Phi$, $\Delta\Theta$ and $\Delta\Psi$ are angles in arcseconds. Φ is a rotation about the Z-axis (yaw), Θ is about the intermediate y (pitch), and Ψ is about the final x$'$ axis (bank or roll). Positive angles are given by the right-hand rule. The first 3 columns of the positioning matrix have units μm/mm and the last 3 columns have units μm/arcsecond. Although this matrix was derived with the Euler rotation transformation, it can be seen that the first 3 columns are proportional to the direction cosines, and the last 3 columns are proportional to the torque vector equation given above.

Positioning Accuracy: In order to maintain the imaging specifications for the f/5.4 wide field modes, some of us anticipated that we would be required to actively control the primary mirror axis with respect to the corrector and rotator axes as a function of elevation. Fortunately this is not the case. In particular, we find acceptable differential defocus from tilt induced gravitation flexure (sections 7.2 and 7.3) and negligible differential distortion due to secondary miscollimation (section 7.4.2). The expected uncertainty between the optical and mechanical axes of the primary mirror can be tolerated (section 7.5) as can the gravitational flexure of the corrector cell (section 7.7.3).

The initial alignment between the primary mirror, corrector, and rotator axes is the only remaining criterion that sets the positioning resolution specification for the hardpoint members. Our budget allows 4 μm of differential distortion (section 5.3.4) and 11 μm of image degradation(section 5.3.3) due to the mechanical alignment of the primary mirror. Using the results of section 7.5, the image degradation budget is consumed by the displacement between the mechanical and optical axes of the primary mirror. Therefore, the hardpoint positioning resolution must allow the mirror to be positioned to about 10% of this error. We can then remove a fraction of the error either empirically based on wide field imaging or by measuring the position of the optical axis with respect to the mechanical center and compensating during the initial alignment.

Hardpoint length changes corresponding to positioning the primary mirror to 10% of the wide-field imaging specifications are:

Motion of primary mirror	Max. hardpoint length change μm	Min. hardpoint length change μm
0.1 mm decenter	57	12
2 arcsec tilt	19	3

Collimation Specification: Although active collimation is achieved by positioning the secondary relative to the primary mirror, it is instructive to calculate the changes in hardpoint lengths that maintain the collimation specification. For all optical modes, 2 arcseconds of primary mirror tilt corresponds to the secondary tilts (shown in section 7.4.1). The table below shows the maximum and minimum length change for the six hardpoints for various motions of the primary mirror which correspond to the collimation specification. The azimuth of the applied motion determines to which individual hardpoint the extensions correspond.

Primary mirror motion	Max. hardpoint length change	Min hardpoint length change
2 arcseconds tilt	19	3
75 μm decenter	43	9
6 μm defocus	4.8	4.8

Positioning Envelope: The hardpoints must have the range required to actively position the mirror throughout an envelope which is a rectangular solid of dimensions 2 mm (cross-lateral, for optical alignment) x 9 mm (elevation: 2 mm alignment + 3 mm gap in the static supports + 1 mm thermal expansion for 30° temperature change over the cell radius + 3 mm compression of the static support rubber with 1g mirror loading) x 10 mm (optic axis: 3 mm rubber compression + 4 mm gap + 3 mm alignment). The positioning envelope has these nonintuitive dimensions because it must accommodate controlled pick-up and put-down of the mirror along -z (for zenith pointing) and -y for horizon pointing. But in the cross-lateral, +z, and +y directions, the hardpoints need only accommodate optical alignment motion. This requires a hardpoint stroke of 11.5 mm. Any motion of the mirror outside of this envelope occurs only in a breakaway condition.

Hardpoint Positioning Specifications:

- Active control of the hardpoint lengths is only required for the initial optical alignment of the telescope and wide field corrector. But once positioned, the hardpoints need not be adjusted as a function of elevation for any of the optical modes.
- The hardpoints will accommodate controlled mirror pick-ups and let-downs at any elevation including horizon pointing.
- Maximum range of hardpoint: $\pm$12 mm (limited by roller screw).

- Maximum positioning volume of the primary mirror is a rectangular solid 2 mm (cross-lateral) x 9 mm (elevation) x 10 mm (optic axis) requiring a hardpoint stroke of 11.5 mm. The nominal mirror operating position is NOT at the center of this volume.
- Hardpoint resolution $\sim 1 \mu$m .
- Control bandwidth: < 1 Hz.
- Because we do not require active positioning during tracking, the velocity limit is somewhat arbitrary. Consider that at a velocity of 30 μm s^{-1} (the LBT specification), the hardpoints will require just over 3 minutes to pick up or set down the mirror.

8 Thermal and Wind Effects on Optical Performance

8.1 Defocus due to Temperature Changes

The simplest of the topics in this section is thermally induced focus changes. McLeod (1995) has worked out general analytic formulae to describe the effects, which we reproduce here. Considering only the primary-secondary mirror separation, the angular defocus caused by a temperature change, ΔT, is

$$\theta = \left[\frac{1}{F_p^2} + \frac{1}{F^2}\right] \frac{\alpha \Delta T L}{D}, \tag{9}$$

where F_p and F are the primary and final focal ratios, α is the coefficient of thermal expansion, L is the primary-secondary spacing and D is the telescope diameter. Since $L \sim F_p L$, and $\frac{1}{F^2} \ll \frac{1}{F_p^2}$, we obtain:

$$\theta \sim \frac{\alpha \Delta T}{F_p}. \tag{10}$$

For the 6.5 meter, $\alpha \sim 12{\times}10^{-6}$ per °C, $F_p = 1.25$ and we arrive at a defocus of $\sim$2.0 arcseconds per °C. We have therefore created a very expensive, but sensitive thermometer! We have company because everyone else who has built a telescope has done the same thing. We have only the additional sensitivity due to our fast primary.

We derive a more general formula for the required secondary refocus due to four terms: (1) expansion of the telescope structure, (2) expansion of the primary mirror, (3) expansion of the secondary mirror and (4) material between the primary mirror vertex and the focal surface (back focal distance).

$$\Delta Z = -\alpha_L L \Delta T_L + \frac{m^2}{m^2+1}\alpha_p f_p \Delta T_p + \frac{(m-1)^2}{m^2+1}\alpha_s f_s \Delta T_s - \frac{1}{m^2+1}\alpha_b b \Delta T_b, \tag{11}$$

where f_p and f_s are the focal lengths of the primary and secondary mirrors, b is the back focal distance, and m is the (transverse) magnification. A positive ΔZ corresponds to moving the secondary away from the primary. An approximate summary of secondary defocus terms can be obtained by setting $\alpha_L = 12{\times}10^{-6}$ per °C, $\alpha_p = 2.8{\times}10^{-6}$ per °C, $\alpha_s = 2.8{\times}10^{-6}$ per °C or $\sim$0, and $\alpha_b = 10{\times}10^{-6}$ per °C, a weighted average of the primary and cell. We obtain:

Equivalent Secondary Defocus
$\Delta Z/\Delta T$ (μm/°C)

Source	f/5	f/9	f/15
Optics Support Structure	-75	-83	-88
Primary	22	22	23
Secondary	0	-3	0
Back Focus	-1	-0.3	-0.2
Total	-54	-64	-65

These equivalent secondary movements are about 20 times larger for a 1 °C temperature change than allowed by our image quality specifications. Monitoring the temperature of the telescope at the level of 0.05°C is required to maintain good focus.

8.2 Thermal Control of the Primary and Secondaries

8.2.1 Introduction

This section will detail the thermal specifications for the primary and secondary mirrors as they relate to optical performance of the telescope and provide a brief explanation of their origins. The details of the thermal systems themselves are beyond the scope of this document (see Miglietta 1992 for a description of the primary mirror thermal control system and Gray 1996 for the f/9 thermal system).

8.2.2 Background

Thermal Distortion of Mirrors If a mirror is figured at temperature T_0, but then operated at temperature T, every length of the mirror l_0 becomes l:

$$l = l_0(1 + \alpha(T - T_0)) \tag{12}$$

where α is the coefficient of thermal expansion (CTE). Under isothermal conditions, the shape of the mirror is preserved but the focal length changes slightly. If, however, there are variations in the CTE and/or temperature, then the shape changes such that:

$$\Delta l \simeq [(T - T_0)\Delta\alpha + \alpha\Delta T] \tag{13}$$

The first term in the preceding equation describes the dimensional variation resulting from a non-uniform CTE in the blank when the operating and polishing temperatures are different and isothermal. This term applies to Zerodur as well as E6 blanks. The second term describes the dimensional variation that occurs when the CTE is uniform but temperature variations within the blank are present.

Mirror Seeing When a mirror is not at ambient temperature, it can create convection-driven air turbulence. Light refraction at the boundaries of air currents of different temperatures produces mirror seeing. The worst mirror seeing is found over a zenith pointing mirror that is warmer than ambient. Forcing air to flow across the mirror surface reduces the scale of turbulence at refractive boundaries, and improves mirror seeing by making the turbulence more laminar. Such an air flow can be produced by tilting the mirror away from zenith and by opening the enclosure to allow adequate circulation of ambient air.

Many variables contribute to mirror seeing. Perhaps the only way to quantify the mirror seeing is empirically. Raccine et al. (1991) found that when the primary of the 3.6 m CFHT is warmer than ambient and pointed near zenith, the contribution to the FWHM image size, F, from mirror seeing is:

$$F \sim 0.40 \cdot \Delta T_m^{\frac{6}{5}} \tag{14}$$

where F is in arcseconds and ΔT_m is the difference between the mirror and ambient temperatures. Other work corroborates these results (see e.g., Lowne 1979, Gillingham 1983, and Angel 1987).

8.2.3 Thermal Control Specifications

The use of thermal control to maintain excellent image quality relies on four elements: 1) insure that the mirror blank has a short thermal time constant so it can be forced to follow ambient temperature variations precisely, 2) open the telescope enclosure as much as possible to ambient air, 3) actively sense and eliminate temperature gradients within the blank, and 4) insure that the blank is manufactured from glass with the lowest possible CTE variations.

The performance of the primary and secondary thermal ventilation systems is specified by an r_0=214 cm structure function at each optical surface (see sections 6.1.1 and 6.2.1). In addition, each optic can scatter no more than 3% of the light outside the seeing disk at a 350 nm wavelength (see section 4.1). We set 1% scattering as the contribution from thermal nonuniformities. Using equations (4) and (5) we then find that $\delta(t)/t \sim 100$ nm m^{-1} for the primary and secondary mirrors (where $\delta(t)$ is the value of the structure function at the scale of the mirror thickness t).

Additionally, the telescope seeing specification is 0.06″ FWHM (section 5.2) implying a contribution no larger than 0.04″ FWHM (combining by the 5/3 power) at the entrance pupil for either mirror. This is equivalent to 0.17″ and 0.27″ FWHM at the surface of the f/5 and f/9 secondaries, respectively).

Mirror Blank Temperature Variations As noted above, for a mirror substrate with non-zero CTE, temperature variations within the blank cause mirror surface distortion. Setting the second term equal to the (entire) structure function specification gives:

$$\Delta T \sim \frac{2}{\alpha} \cdot \frac{\delta(t)}{t} \tag{15}$$

where $\alpha = 2.9\times10^{-6}$ °C^{-1} for E6 glass. We don't divide the structure function into two terms because this is an order of magnitude estimation. This specification implies controlling temperature variations to within 0.1 °C for both the primary and secondary mirrors. Empirical work suggests the same conclusion (e.g., Siegmund et. al. 1986 and Pearson et al. 1986).

More recently though, finite element models of honeycomb mirrors for the LBT project suggest that the thermal specifications for honeycomb borosilicate mirrors are:

- radial temperature gradient less than 0.25 °C.
- faceplate-to-honeycomb gradient less than 0.30 °C.
- random temperature variations less than 0.15 °C P–V.

The Zerodur f/5 secondary blank is insensitive to thermal gradients.

Mirror Blank CTE Variations The variation of CTE within a mirror blank limits the difference between the polishing and operating temperatures. Since our mirrors are polished near a temperature of 20 °C and the lowest temperature we expect to run the telescope at is $\sim$ -10 °C, we encounter a span of 30 °C. From equation (13) we derive:

$$\Delta\alpha \sim \frac{2}{(T_0 - T)} \cdot \frac{\delta(t)}{t} \tag{16}$$

Thus, we require an RMS CTE variation of $\sim 7\times10^{-9}$ °C^{-1} to meet the specification over the full temperature range. The E6 casting process achieves an P–V CTE variation of $\sim 9\times10^{-9}$ °C^{-1}. The P–V variation of the f/5 Zerodur blank was measured by Schott to be about 2×10^{-8} °C^{-1}. These numbers meet or nearly meet the specification.

Mirror Seeing and Tracking the Ambient Temperature Both the primary and secondary mirrors must have time constants near 30 minutes in order to track the ambient temperature cooling rates on mountaintops. The accuracy of the thermal control servo is derived from equation (14) and the temperature changes observed at the MMT site. Setting the image blur from local seeing at the primary and secondary mirrors to be $0.04''$ at the entrance aperture, we obtain the results shown in the table below.

Maximum Blank Thermal Gradients and Deviations from Ambient Temperature

Mirror	Max Image FWHM at optic	Diff. from Ambient (°C)	Gradient (°C)
Primary	0.04	0.15	0.1
f/5	0.17	0.50	∼1.0
f/9	0.27	0.70	0.1
f/15	0.40	1.00	TBD

The specifications relax when the mirrors are tilted away from zenith and when the mirrors are cooler than ambient. The gradient in the Zerodur f/5 secondary is set by the allowable deviations from the ambient temperature.

The air mass per unit time, $\dot{m}_a$, that must be delivered to a mirror to control its temperature is (Cheng and Angel 1986,1988):

$$\dot{m}_a = \frac{M c_g}{\tau c_a \eta} \tag{17}$$

where M is the mass of the mirror, c_g is the specific heat of the glass ($\sim$ 730 J kg^{-1} C^{-1}), c_a is the specific heat of air (1004 J kg^{-1} C^{-1}), τ is the thermal time constant and η is the coupling efficiency between the forced air and the glass.

The table below summarizes the estimated thermal ventilation parameters for the MMT optics. Air flow rates were calculated for the altitude of Mt. Hopkins at 20 °C where the air density is lowest and flow rates are maximized. Calculations are for a mirror time constant of 30 minutes, and the convective coupling efficiency between the air flow and glass structures is assumed to be 0.6 (from Cheng and Angel). **The last column estimates the heat removed from the mirror only** for maximum slew rates expected near sunset (2 °C hr^{-1}). In general, mountain top slew rates are no greater than 0.25 °C hr^{-1}.

Required MMT Optics Ventilation

Mirror	Mass (kg)	c_g (J kg^{-1} C^{-1})	Air Flow Total (kg s^{-1})	Air Volume Total (m^3 s^{-1}, CFM)	Air Volume per cell (cells, l s^{-1})	Heat Removal (2 °C hr^{-1}) (W)
Primary	8500	740	5.8	6.5, 13400	1020, 6.5	3500
f/5	288	730	0.20	0.22, 465	305, 0.83	102
f/9	77	740	0.05	0.06, 127	168, 0.35	32

We can now itemize the thermal specifications related to tracking of mirror temperature to ambient (some additional specifications are gleaned from the LBT specifications – Hill 1995). The jet-ejector ventilation system that achieves these goals is described by Miglietta (1992).

- Temperature variations in glass of non-zero CTE shall not deviate from a best-fit linear distribution across the mirror by more than 0.1 °C P–V under conditions where the ambient temperature is changing by up to 0.25 °C hr^{-1}.
- The mean temperature of the primary mirror shall not differ from the ambient temperature by more than 0.15 °C under slew conditions of up to 0.25 °C hr^{-1} (see Table1 for the secondaries).
- The cooling system shall have the capacity to slew the mirror by 2 °C hr^{-1} but is not required to maintain the uniformity specification at that rate.
- Transient temporal variations over a 10 minute interval of in the air temperature exiting the nozzles are allowable provided the following conditions are met:

  In the telescope cell, three effects contribute to the temperature variations in the mirror, and each must be controlled to ±0.03 °C (assuming they add in quadrature): 1) spatial gradients arising from time constant variations, 2) ventilation system errors, and 3) coolant loop temperature variations (although saw-tooth variations of up to 1 °C are tolerated for periods of 5 minutes (which is much less than the time constant of the mirror).
- The maximum pressure difference between any two points on the mirror backplate must be less than 40 Pa. Temporal variations in pressure must be less than ±10 Pa. The mean pressure on the backplate must not differ by more than 40 Pa from the mean local ambient pressure.

Temperature Measurement System The mirror cell computer monitors the temperature of the mirror and cell interior via thermocouples distributed throughout the mirror and cell. The specifications for this system are:

- Sensor: type T thermocouple (copper-constantan).
- Absolute accuracy and linearity: ±0.01 °C.
- Differential accuracy: 0.01 °C.
- Resolution: 0.005 °C.
- Operating range: -25 to +30 °C.

8.3 Wind Effects

8.3.1 Overview

The wind vibrates (and may distort) the optics on their support systems and vibrates the optics support structure (OSS). Here, we present the vibration error budget, summarize the expected rigid-body response of the primary mirror on its support system, and estimate the mirror figure distortion due to uncorrected dynamic wind forces. In general, wavefront tilts and the resulting image motions degrade the image quality well before decollimation becomes an issue. We discuss the implications of the SG&H analysis of the OSS's sensitivity to wind loads. The SG&H results are summarized in Section 7.2.

Due to the inherently stiff mechanical structure of the honeycombed primary mirror, it naturally resists distortion in the presence of winds. The pneumatic force support system isolates the mirror from the [relatively flexible] cell with a bandwidth of 5 Hz (inner servo loop). However, despace errors and wavefront tilt arise from uncorrected solid-body vibration induced by wind turbulence. In addition, the uncompensated dynamic wind force distorts the mirror against the stiff hardpoints.

8.3.2 Optical Vibration Error Budget

The error budget for the primary mirror is given in Section 6.1; it includes a term for wind forces of magnitude $0.050''$ FWHM, corresponding to an r_0 of 214 cm. The wind error budget for the secondary mirror is given in Section 6.2; it also is $r_0 =$ 214 cm, but as discussed in Section 6.2, the scaling to total image degradation is more favorable by the pupil demagnification factor (see Section 6.2 for a detailed discussion). Thus, the resulting image degradation is a factor of 4.2 to 9.9 smaller than the $0.050''$ FWHM allotted for the primary. Note, however, that this term is not discussed here. Motion of the OSS falls under the heading of secondary alignment and focus (see Section 5), which has a total magnitude of $0.090''$ FWHM, corresponding to an r_0 of 112 cm.

Piston, tilt, and decenter vibrations must be considered. To first order, piston vibrations do not affect the diffraction performance of a telescope with a stiff single mirror because the entire field is de-phased coherently. Therefore, the piston tolerance is given by image blur resulting from geometric despace errors.

Wavefront tilt is caused by tilting or decentering the optics. Following a reflection at the tilted primary mirror, the wavefront tilts by twice the surface tilt, independent of the secondary. To produce the same wavefront tilt at the secondary, the secondary tilt must be larger by the (tranverse) pupil demagnification (given in Section 6.2).

The amount of secondary or primary motion required to produce an image motion of $0.05''$ is tabulated below.

Primary and Secondary Motions for Image Motions of $0.05''$

	Primary Tilt (arcsec)	Primary Decenter (microns)	Sec. Tilt (arcsec)	Sec. Decenter (microns)
f/5	0.025	2.1	0.11	2.7
f/9	0.025	2.1	0.17	2.4
f/15	0.025	2.1	0.25	2.3

These motions, to the extent that they cannot be guided out, set a much tighter limit than the collimation tolerances in Section 7.4 and 7.5. In Sections 7.4 and 7.5 we assume that the collimations changes are slow enough that image motion can be guided out.

8.3.3 Atmospheric Image Motion

Before we derive an error budget it is interesting to calculate the image motions that the atmosphere will induce. This calculation is for comparison only; our error budget is based on other considerations. John Hill gives an equation relating (1D) RMS image motion induced by the atmosphere, $\delta\theta$ (in arcsec), the telescope diameter in meters, D, and r_0 (at 0.5 μm) in meters:

$$\delta\theta = 0.043 D^{-1/6} r_0^{-5/6} \quad arcsec \tag{18}$$

.

For a 6.5 m telescope and $r_0 = 45$ cm, we expect $0.06''$ image motion.

8.3.4 Primary Mirror Vibration and Figure Distortion

The approximate wind vibration response of the primary mirror resting on its support system has been estimated (West & Martin 1995). This section briefly summarizes that work. A realistic wind turbulence power spectral density (PSD) was obtained from recent wind literature and was parameterized for conditions appropriate for Mt. Hopkins. It was converted into a wind drag force PSD, $S_D(\nu)$. The drag PSD is related to the displacement response PSD $S_x(\nu)$ by the square of the mechanical admittance $H(\nu)$ of the primary mirror on its support system. $H(\nu)$ is given by the

harmonic oscillator response to the Stewart platform hardpoint members combined with the servo and damping response of the air support system. For a one-dimensional wind turbulence, the RMS vibration response, X_{RMS}, of the primary mirror over bandwidth ν_2 - ν_1 is given by:

$$X^2_{RMS} = \int_{\nu_1}^{\nu_2} H^2(\nu) S_D(\nu) d\nu \tag{19}$$

To estimate the effects of turbulence decorrelation and torque moments introduced by pressure gradients over a 6.5 m aperture, a three dimensional analysis was performed. The estimated RMS motions of the primary mirror for hardpoints with a stiffness of 80 N μm^{-1} (the MMT hardpoints have since been determined to have a stiffness of 95 N μm^{-1}) and the observed damping of the Air Force 3.5 m support system (which incorporates pneumatic supports similar to the 6.5 m MMT) are shown in the table below. The vibrations shown are for the worst case with an unshielded primary mirror pointing into the wind.

RMS Primary Mirror Motions
Versus Mean Wind Speed

	Error Budget	Wind Speed	
Motion		6.7 m s^{-1}	22 m s^{-1}
Piston	3.5μm	0.087 μm	1.35 μm
Decenter	0.89μm	0.31 μm	4.8 μm
Tilt	0.011″	0.003″	0.048″

The primary error budget allows an 0.050″ FWHM contribution to the image from wind forces on the primary mirror. This translates into a 0.021″ RMS contribution. The error budget (for tilt and decenter) shown for the primary mirror on its support system is exceeded when the telescope points into a mean wind of 11 m s^{-1} (assuming the vibration ampitudes scale as V$^{2.3}$). The defocus resulting from the piston term is a small fraction of the total collimation error budget (see Section 7.4).

The correction of rigid-body forces and moments on the mirror (by the outer-loop servo) removes mirror figure distortion arising from the mean wind static pressure. However, the correction of the dynamic forces on the mirror is incomplete. This results in figure distortion as the wind turbulence pushes the mirror into the stiff hardpoints. Using an FEA model, this distortion was estimated by reacting the uncorrected dynamic wind force on the mirror against the six hardpoints (Cuerden 1998) . The resulting surface-error structure function was compared to the wind error budget (r_o = 214cm). The mirror figure meets specification in mean wind velocities up to 13 m s^{-1}.

8.3.5 Optics Support Structure (OSS)

SGH estimated the deflections of the secondary mirror connection caused by wind loading of the OSS. They looked only at the deflection caused by a steady wind drag with a velocity of 18 m s^{-1} (40 mph). Wind turbulence vibrations were not calculated. The SG&H results are summarized in Section 7.2. If the telescope is initially perfectly collimated, the resulting secondary deflections remain within the secondary collimation error budget in Section 7.4, but this error budget doesn't include direct image motion contributions. In order to maintain complete consistency, we should revise Section 7.4 to include a term for direct image motion due to wind forces on the OSS. Instead, we calculate what wind velocity will produce an 0.05″ FWHM contribution to the image blur. When added in quadrature to the other collimation errors, the wind term will increase the total decollimation image blur by 14%.

f/5 Secondary Mirror Motions from a 18 m s^{-1} Wind on the OSS (from section 7.2)

Motion	Error Budget	Wind Deflections
Piston	3.5μm	0.81 μm
Decenter	2.7μm	39 μm
Tilt	0.11″	1.75″

The error budget is derived (approximately) by equating the FWHM contribution to image blur and the wind deflection. We assume that OSS distortion is proportional to the square of the wind velocity. Therefore, the tilt and decenter specifications are exceeded for a 5 m s^{-1} wind. The piston contribution to the defocus is small. However, 5 m s^{-1} is a conservative velocity limit, since in order to assess the true impact of wavefront tilt on image quality, a power spectral analysis would have to be performed on the wind-induced OSS vibrations and then related to the mechanical admittances of the telescope mount and hexapod (i.e., some of the image motion will be removed with the mount servo).

9 Reflectivity and IR Performance

9.1 Infrared Performance

The following was provided by George Rieke.

The overall concept for the MMT (and the Magellan and LBT) infrared configurations is in accordance with the precepts for high performance infrared astronomy developed at the University of Arizona (Low and Rieke 1974). The design will provide an effective telescope emissivity of 3% (4% for Magellan and the LBT) and agile infrared secondary mirrors. In this concept, thermal backgrounds are rejected by a cold Lyot stop that is slightly oversized relative to the secondary mirror. The secondary is undersized so that the extreme rays reaching the detector are from cold sky rather than from warm telescope structure. Because the secondary is far from the detector, Fresnel diffraction occurs off its edges, resulting in stronger rejection of off-axis backgrounds than can be achieved by the Lyot stop alone. Modulation is carried out by chopping the secondary mirror over a small angle. The telescope has a small central obscuration and low emissivity coatings to minimize its emission into the beam.

The converted MMT, the Magellan telescope, and the LBT will be further optimized for thermal infrared performance as described by Rieke (1987). Good secondary agility requires a small primary f/ratio, but diffraction limited imaging in the face of the coma induced by tilting the secondary favors a large f/ratio. The selection of an f/1.25 primary represents a careful balancing of these two contradictory requirements; the strehl ratio at 10μm at maximum secondary tilt angle is ¿ 0.92. Through raytrace analysis of a number of possible instruments, it was determined that a Cassegrain f/ratio of 15 allows good imaging, as well as an agile secondary mirror.

10 Useful Related Documents (Annotated References)

1. Angel, J.R.P, Cheng, A.Y.S., and Woolf, N.J. 1985,"Steps toward 8m honeycomb mirrors VI: thermal control", Proc SPIE v571, p

2. Angel, J. R. P. 1987,"Designing 8m mirrors for the best sites", in Identification, optimization, and protection of optical telescope sites, ed. R.L. Mills, O. G. Franz, H.D. Ables, C.C. Dahn, p. 167-176, Flagstaff: Lowell Observatory.

3. J. Antebi, September 1992, Communication 89057, "Conversion of MMT to 6.5 m Telescope: Study of Actuator Tilts as OSS Changes Elevation"

4. J. Antebi, September 1992, Communication 89057, "Conversion of MMT to 6.5 m Telescope: Frequency and Deflection Analyses of OSS, Yoke and Tower, Summary of Results

5. J. Antebi, October 1994, Communication 93072, "Conversion of MMT to 6.5 m Telescope: Relative Deflections of Corrector Cell"

6. BCV Report No. 1, "Mirror Blank 6.5 m diameter f/1.25," Milano Italy, December 1989.

7. BCV Report No. 4 rev. 0, "Mirror Blank 6.5 m diameter f/1.25: Improvement of Optimization Procedure," Milano Italy, December 1991.

8. BCV Report No. 6 rev. 0, "Mirror 6.5 m F/1.25: Finite Element Model," Milano Italy, November 1994.

9. BCV report No. 7 rev. 0, "Mirror 6.5 m F/1.25: Axial and Lateral Supports Optimization," Milano Italy, December 1994.

10. BCV Report No. 105, "Mirror blank 8.0 diam F1 axial support optimization", Feb. 29, 1988, BCV progetti s.r.l.

11. BCV report No. 113, "Honeycomb-meniscus mirror blank comparison", Milano May 15, 1989, BCV progetti s.r.l.

12. J.H. Burge and D.S. Anderson, March 1994, SPIE Proceedings 2199, "Full Aperture Interferometric Test of Convex Secondary Mirros Using Holographic Test Plates"

13. J.H. Burge and H.B. Martin, February 1993, "Tolerances for MMT Primary"

14. Cheng, A. Y. S. and Angel, J. R. P. 1986, "Steps towards 8m honeycomb mirrors VIII: design and demostration of a system of thermal control", Proc SPIE v628, p536.

15. Cheng, A.Y.S and Angel, J.R.P. 1988, "Thermal stabilization of honeycomb mirrors", Very Large Telescopes and Their Instrumentation, ed. M.H. Ulrich, p467-477 (Munich:ESO).

16. Cuerden, B., June 24, 1996, "Stress analysis of mirror at hardpoint", UA internal memo.

17. Cuerden, B. August 7, 1996, "MMT/Magellan cell counterweight drawing completion", UA internal memo.

18. Cuerden, B. "Wind Distortion of the MMT Primary and f/9 Secondary Mirrors," MMTO Technical Memo 98-1, 1998.

19. D. Fabricant, February 1993, memo: "Tolerances for the 6.5m Primary Figure"

20. D. Fabricant, September 1993, memo: "Optical Description of MMT F/5.4 Corrector"

21. D. Fabricant, September 1994, memo: "Final ADC Prism Configuration"

22. D. Fabricant, April 1995, "Fabrication Specifications for the SAO Wide-Field Corrector Elements"

23. D. Fabricant, November 1999, "Polishing Specifications for the Converted MMT f/5 Secondary Mirror"

24. R. Fata and D. Fabricant, July 1993, SPIE Proceedings 1998, "Design of a Cell for the Wide-Field Corrector for the Converted MMT"

25. R. Fata, November 1993, "MMT F/5.4 Secondary Mirror Fabrication Specification", S-MMTC-300, Revision 1

26. R. Fata and D. Fabricant, March 1994, SPIE Proceedings 2199, "The Design an Support of the 1.7m Secondary Mirror for the MMT Conversion"

27. Gillingham, P. R. 1983, "Seeing measurements at the Anglo-Australian telescope", Proc. SPIE 444, p 165.

28. P. Gray, J.M. Hill, W.B. Davison, S.P. Callahan and J.T. Williams, March 1994, SPIE Proceedings 2199, "Support of Large Borosilicate Honeycomb Mirrors"

29. Gray, P.M, West, S.C., and Gallieni,W. 1996 "Support and actuation of six secondaries for the 6.5 m MMT and 8.4 m LBT telescopes", Telescopes of Today and Tomorrow, Proc. ESO/SPIE, In press.

30. J.M. Hill April 1994, memo: "Dimensions for Large Borosilicate Mirrors" (URL: `ftp://as.arizona.edu/pub/mirror/honeycomb.ps`)

31. J.M. Hill September 1993, LBT Technical Memo UA-93-06, "Infrared Secondaries: The Meaning of F/15"

32. J.M. Hill, August 1994, LBT Technical Memo UA-94-01, "Error Budget and Wavefront Specifications for Primary and Secondary Mirrors"

33. Hill, J. M. 1995, "Mirror support system for large honeycomb mirrors II/R", UA-95-02.

34. Lloyd-Hart, M. 1990, "System for precise temperature sensing and thermal control of borosilicate honeycomb mirrors during polishing and testing", Proc SPIE v1236, 844.

35. F.J. Low and G.H. Rieke, 1974,"The instrumentation and techniques of infrared photometry", in Methods of Experimental Physics, Vol 12, part A, Astrophysics–Optical and Infrared, ed. N. Carleton, Academic Press.

36. Lowne, C. M. 1979, Mon. Not. Roy. Astron. Soc., v188, 249.

37. B. McLeod, February 1995, memo: "Focus vs. Temperature at the 48 Inch and the 6.5 meter" (URL: `http://cfa-www.harvard.edu/~ bmcleod/temperature.ps`)

38. Miglietta, L. 1992, "Air-air ejector for large mirror temperature control: numerical simulations and experimental data", Progress in Telescope and Instrumentation Technologies, Proc. ESO, Garching, 361-364.

39. Miglietta, L., and Callahan, S. 1996, "The position actuators of the 6.5m borosilicate honeycomb primary mirrors", SPIE Annual Conference, v2865, in press.

40. B. Olbert, J.R.P. Angel, J.M. Hill and S.F. Hinman, March 1994, SPIE Proceedings 2199, "Casting 6.5 Meter Mirrors for the MMT Conversion and Magellan"

41. Pearson, E., Stepp, L., Wong, W-Y, Fox, J., Morse, D., Richardson, J., and Eisenberg, S. 1986, Proc. SPIE v628, 91.

42. Racine, R., Salmon, D., Cowley, D., and Sovoka, J. 1991, "Mirror, dome, and natural seeing at the CFHT", PASP v103, 1020.

43. G. Rieke, September 1987 memo, "Infrared configuration for 8 meter telescopes with fast primaries", (report to Magellan Project science advisory committee).

44. J. Ruze, 1966, Proc. I.E.E.E., 54, 633

45. Schott Glaswerke, February 1995, "QC Certificate for f/5 Secondary", OT-0295099

46. Siegmund, W. A., Mannery, E. J., Radochia, J., and Gillet, P. E. 1986, Proc. SPIE, v628, 377.

47. Simpson, Gumpertz and Heger, July 1990, report: "MMT Conversion, Final Conceptual Design with Inverted Serrurier Truss"

48. D. Stewart 1965, "A Platform with Six Degrees of Freedom", Proc. Instr. Mech. Engr. 180, 371-386.

49. Tomelleri, R. February 1996, "MMT Conversion Project – M1 mirror hardpoints – acceptance inspections", Studio Tecnico Tomelleri, Verona Italy.

50. S.C. West and H.M. Martin, June 1995 "Approximate wind disturbance of the MMT 6.5 m primary mirror on its supports", MMT Technical Report 28, University of Arizona – Smithsonian Institution.

51. West, S.C., March 1996a, "A hardpoint length calculator for the MMT conversion", MMT Conversion Technical Memorandum No. 96-1, University of Arizona – Smithsonian Institution.

52. West, S. C., 1996b "Hardpoint platform matricies for the MMT 6.5 -m primary mirror cell", unpublished memo.

53. West, S. C., 1997, "Polishing Specifications for the MMT f/9 Secondary Mirror," MMT Technical Memo 97-2, Oct. 9, 1997.

54. West, S.C., Callahan, S., Chaffee, F. H., Davison, W., DeRigne, S., Fabricant, D., Foltz, C.B., Hill, J.M., Nagel, R.H., Poyner, A., and Williams, J.T. 1996, "Toward first light for the 6.5-m MMT telescope", Optical Telescopes of Today and Tomorrow, SPIE/ESO v2871, in press.

55. J.T. Williams, February 1992, memo: "6.5 m Instrument Rotator Performance Goals and Specifications"